Med

Article

Efficacy and safety of adjuvant TTFields plus pembrolizumab and temozolomide in newly diagnosed glioblastoma: A phase 2 study

Graphical abstract

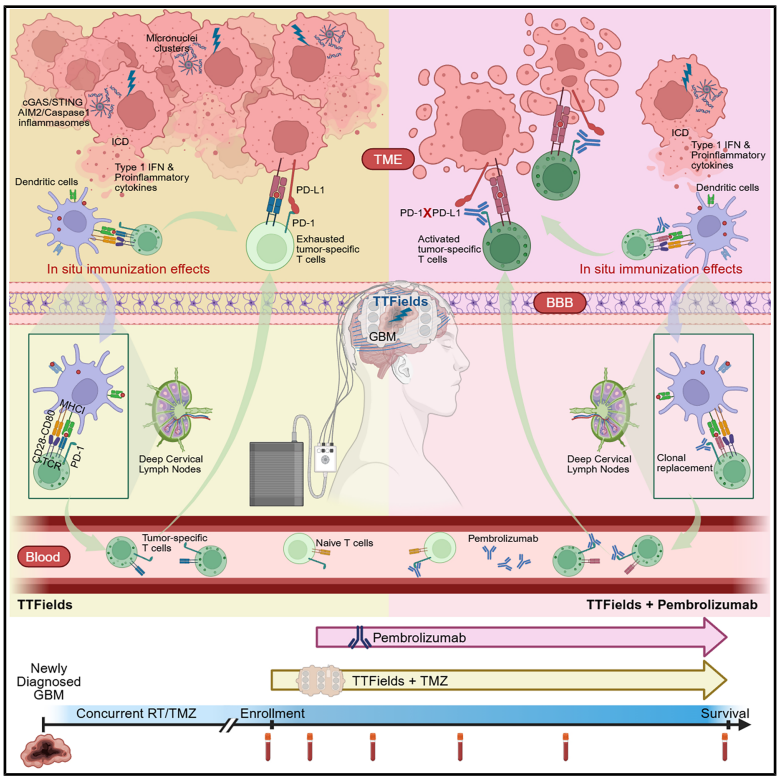

Highlights

- TTFields plus pembrolizumab and TMZ improved survival in newly diagnosed GBM
- The triple regimen improved survival in patients with biopsy-only tumor
- The triple regimen enhanced anti-tumor immunity, especially in biopsy-only patients
- The triple regimen was generally well tolerated

Authors

Dongjiang Chen, Son B. Le, Ashley P. Ghiaseddin, ..., Adam O'Dell, Maryam Rahman, David D. Tran

Correspondence

david.tran@med.usc.edu

In brief

Chen et al. investigated the efficacy of TTFields plus pembrolizumab and TMZ in newly diagnosed GBM. The triple regimen improved survival and enhanced anti-tumor immunity, especially in patients with bulky tumors. These findings suggest that TTFields can augment the efficacy of immune checkpoint inhibitors in GBM and potentially other tumors.

Translation to Patients

Chen et al., 2025, Med 6, 100708
September 12, 2025
Published by Elsevier Inc.
https://doi.org/10.1016/j.medj.2025.100708

CellPress

Please cite this article in press as: Chen et al., Efficacy and safety of adjuvant TTFields plus pembrolizumab and temozolomide in newly diagnosed glioblastoma: A phase 2 study, Med (2025), https://doi.org/10.1016/j.medj.2025.100708

Med

CellPress
OPEN ACCESS

Article

Efficacy and safety of adjuvant TTFields plus pembrolizumab and temozolomide in newly diagnosed glioblastoma: A phase 2 study

Dongjiang Chen,[1,2,6] Son B. Le,[1,2,6] Ashley P. Ghiaseddin,[3,6] Harshit Manektalia,[1,2] Ming Li,[4,5] Adam O'Dell,[1,2] Maryam Rahman,[2] and David D. Tran[1,2,5,7,*]

[1]Division of Neuro-Oncology, Department of Neurosurgery, Keck School of Medicine of USC, Los Angeles, CA 90033, USA
[2]USC Brain Tumor Center, University of Southern California, Los Angeles, CA 90033, USA
[3]Department of Neurosurgery, University of Florida, Gainesville, FL 32611, USA
[4]Department of Population and Public Health Sciences, Keck School of Medicine of USC, Los Angeles, CA 90033, USA
[5]USC Norris Comprehensive Cancer Center, Keck School of Medicine of USC, Los Angeles, CA 90033, USA
[6]These authors contributed equally
[7]Lead contact
*Correspondence: david.tran@med.usc.edu
https://doi.org/10.1016/j.medj.2025.100708

CONTEXT AND SIGNIFICANCE Glioblastoma (GBM) is an aggressive brain cancer with a poor prognosis, and survival for patients with inoperable GBM is especially dismal. While immune checkpoint inhibitors (ICIs) have shown success in other cancers, their effectiveness in GBM has been limited due to the tumor's profoundly immunosuppressive microenvironment. In this study, the researchers investigate the use of TTFields, an electric field treatment known to induce an *in situ* immunization effect against GBM, alongside pembrolizumab, an anti-PD-1 ICI, in newly diagnosed GBM patients. This study confirms that the use of TTFields in conjunction with pembrolizumab enhances immune recognition and anti-tumor immunity, significantly improving PFS and OS, particularly in patients with biopsy-only tumor. These findings suggest that TTFields can augment ICI efficacy, offering a promising new treatment strategy for GBM.

SUMMARY

Background: Immune checkpoint inhibitors (ICIs) have shown limited success in glioblastoma due to the tumor's profoundly immunosuppressive microenvironment. Tumor treating fields (TTFields), a non-invasive electric field therapy, activate the type I interferon (T1IFN) pathway via DNA sensor-dependent inflammasomes, promoting *in situ* immunization against glioblastoma.

Methods: In this phase 2 study (this study was registered at ClinicalTrials.gov: NCT03405792), 31 newly diagnosed glioblastoma patients were enrolled post-chemoradiation to evaluate synergy between TTFields, pembrolizumab, and temozolomide. The primary endpoint was progression-free survival (PFS) compared to case-matched controls treated with TTFields and temozolomide alone. Secondary endpoints included overall survival (OS), response rate, safety, and immune correlates assessed through single-cell transcriptomics and T cell clonotyping of blood and tumor samples.

Findings: Among 26 patients treated per protocol, the median PFS was 12.0 vs. 5.8 months in controls (HR 0.377, 95% CI 0.217–0.653; $p = 0.0026$), and the median OS was 24.8 vs. 14.6 months (HR 0.522, 95% CI 0.301–0.905; $p = 0.0477$). Patients undergoing biopsy had longer PFS (27.2 vs. 9.6 months; HR 0.37, 95% CI 0.16–0.85; $p = 0.014$) and OS (31.6 vs. 18.8 months; HR 0.4, 95% CI 0.17–0.92; $p = 0.023$) compared to maximal resection. Severe adverse events constituted 7.5% of treatment-related toxicities. TTFields promoted clonal T cell expansion via a T1IFN-driven trajectory, while pembrolizumab supported adaptive replacement of these clones, sustaining T cell activation and memory formation, especially in biopsy-only patients.

Conclusions: These findings demonstrate synergy between TTFields and ICIs, particularly in patients with high tumor burden, and support further study in larger trials.

Funding: This work was supported by a grant from Novocure.

Please cite this article in press as: Chen et al., Efficacy and safety of adjuvant TTFields plus pembrolizumab and temozolomide in newly diagnosed glioblastoma: A phase 2 study, Med (2025), https://doi.org/10.1016/j.medj.2025.100708

INTRODUCTION

The survival outlook for glioblastoma (GBM) remains bleak, despite aggressive treatment composed of maximal surgical resection, concomitant chemoradiation, adjuvant temozolomide (TMZ), and tumor treating fields (TTFields). The median overall survival (OS) is 20.9 months, and the 5-year survival rate stands at a mere 13%.[1] For patients with inoperable tumors, the prognosis is considerably worse, with median OS of less than 12 months.[2–4] This stark reality emphasizes an imperative need for new therapeutic approaches to improve outcomes, particularly for patients harboring high tumor burdens beyond the scope of safe surgical excision.

While immune checkpoint inhibitors (ICIs) like anti-programmed cell death protein 1/programmed cell death ligand 1 (PD-1/PD-L1) monoclonal antibodies have shown success in many solid tumors, they show limited efficacy in GBM, despite high intratumor expression of PD-L1.[5–9] The mechanisms for this failure are complex, including GBM's low mutation burden, extensive molecular heterogeneity and immune escape signals, and a profoundly immunosuppressed or "cold" tumor microenvironment (TME), characterized by a dearth of tumor-infiltrating lymphocytes (TILs) and dendritic cells (DCs) and an abundance of immunoinhibitory cells like regulatory T cells and myeloid-derived suppressor cells (MDSCs).[10–12] Current strategies focused on inducing peripheral cytotoxic T cell responses alone have met with limited success, indicating that potent systemic immune activation may not suffice to reverse the cold TME to enhance ICI efficacy.[11] Consequently, recent efforts have pivoted to directly target the TME. This includes the use of intraoperative, intracavitary, or implantable reservoirs for local delivery of therapies such as hyperthermia, oncolytic viruses, or gene therapy to elicit *in situ* immunizing effects with encouraging results when combined with ICIs.[13–15] Nonetheless, there is a critical need for the development of non-invasive, safe, repeated administration strategies capable of directly modulating and sustaining TME stimulation in GBM.

TTFields, approved for newly diagnosed and recurrent GBM,[1] are non-invasive, low-intensity, intermediate-frequency alternating electric fields that elicit anti-neoplastic effects via a plethora of molecular mechanisms.[16] Emerging evidence supports a role for TTFields in inducing immunogenic cell death (ICD).[17,18] We recently reported that TTFields induce focal nuclear envelope disruptions in GBM and other solid tumor cells, causing cytosolic release of large clusters of naked DNA, thereby stimulating cyclic guanosine monophosphate-adenosine monophosphate synthase/stimulator of interferon genes (cGAS/STING) and absent in melanoma 2 (AIM2)/caspase-1 and their cognate inflammasomes to produce local type I interferon (T1IFN) and pro-inflammatory cytokines. This, coupled with free tumor immunogens released by TTFields-induced ICD, creates a non-invasive, on-demand, *in situ* immunization platform for GBM and, potentially, other tumors.[19] Remarkably, in patients with newly diagnosed GBM, TTFields therapy resulted in robust T cell receptor (TCR) clonal expansion via a T1IFN trajectory,[19] and in a phase 3 randomized trial in metastatic non-small cell lung cancer, TTFields plus pembrolizumab significantly extended survival compared to pembrolizumab alone.[20]

To investigate potential synergistic effects of TTFields and pembrolizumab, we conducted a pilot phase 2 study in patients with newly diagnosed GBM, who had either maximal tumor resection or biopsy only and had completed concomitant chemoradiation. The objective was to corroborate TTFields' capacity for *in situ* immunization in the TME by assessing clinical outcomes and peripheral immune dynamics, including in patients with biopsy-only tumors. Conceivably, the higher neoplastic burden in biopsy-only patients is more amenable to the immunizing effects of TTFields plus pembrolizumab. We utilized a multi-omics approach, including paired 5′ single-cell RNA sequencing (scRNA-seq) and TCR sequencing of peripheral blood mononuclear cells (PBMCs) and bulk RNA-seq of enriched T cells, coupled with RNA-seq, whole-exome sequencing (WES), and immunohistochemistry (IHC) of paired primary and recurrent tumors to delineate potential determinants of response and resistance.

RESULTS

Study design and patient demographics and baseline characteristics

The 2-THE-TOP phase 2 trial enrolled newly diagnosed GBM patients who had undergone either maximal tumor resection or biopsy only and completed standard radiation and concurrent TMZ. Eligibility required Karnofsky Performance Status (KPS) $\geq$70%, adequate hematologic and metabolic reserves, and required dexamethasone $\leq$4 mg/day at enrollment. TTFields began with cycle 1 of adjuvant TMZ, with pembrolizumab 200 mg intravenously every 3 weeks added at cycle 2, enabling differentiation of TTFields' early immune effects from the combined effect with pembrolizumab. The primary endpoint was progression-free survival (PFS) compared to historical controls from the EF-14 study,[1] with disease assessment via brain MRI every 9 weeks per the Immunotherapy Response Assessment in Neuro-Oncology (iRANO) criteria.[21] Secondary endpoints included OS, safety, objective responses, and immune signatures using bulk RNA-seq and paired 5′ scRNA-seq and TCR clonotyping of PBMCs and T cell RNA-seq. Preclinical models showed that PBMC changes serve as a surrogate for the TME's immune dynamics along a T1IFN trajectory, later confirmed in TTFields-treated patients,[19] thereby obviating the need for repeated high-risk intracranial sampling. PBMCs were collected at baseline (before TTFields or Pre-TTF), 4 weeks after TTFields (Post-TTF and prior to pembrolizumab at cycle 1), and before cycles 2, 4, 9, 17, and 34, as well as at tumor recurrence. An exploratory objective is to identify TME resistance markers in paired primary and recurrent tumors using RNA-seq, WES, and IHC (Figure 1A).

From 2018 to 2021, 31 eligible patients were enrolled (Figure 1B). Five patients did not receive study treatments—2 withdrew consent without initiating TTFields (1 lost to follow-up) and 3 discontinued TTFields during cycle 1 of TMZ before receiving pembrolizumab (1 lost to follow-up). For evaluability in survival and immune analyses, at least one dose of pembrolizumab was required; the intent-to-treat (ITT) group thus

Please cite this article in press as: Chen et al., Efficacy and safety of adjuvant TTFields plus pembrolizumab and temozolomide in newly diagnosed glioblastoma: A phase 2 study, Med (2025), https://doi.org/10.1016/j.medj.2025.100708

CellPress
OPEN ACCESS

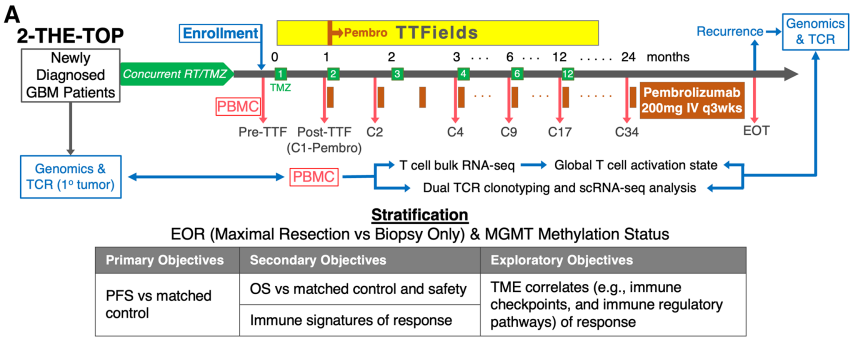

Stratification

EOR (Maximal Resection vs Biopsy Only) & MGMT Methylation Status

Primary Objectives	Secondary Objectives	Exploratory Objectives
PFS vs matched control	OS vs matched control and safety	TME correlates (e.g., immune checkpoints, and immune regulatory pathways) of response
	Immune signatures of response	

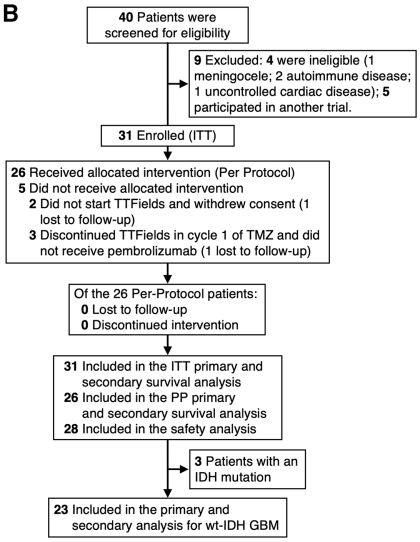

C

Summary of Efficacy

Study Population	N (pts)	mPFS [mo] (95% CI)	mOS [mo] (95% CI)
ITT	31	11.9 (8.83, 16.6)	22.1(13.9, 27)
Per protocol (PP)	26	12 (8.83, 21.1)	24.8 (12.57, 29.57)
Matched controls to PP (EF-14)	56	5.8 (4.37, 7.90)	14.6 (12.93, 17.97)
wt-IDH GBM	23	10.8 (7.4, 16.6)	20.5 (12.5, 25.5)

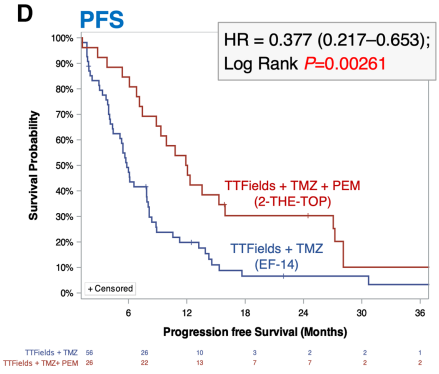

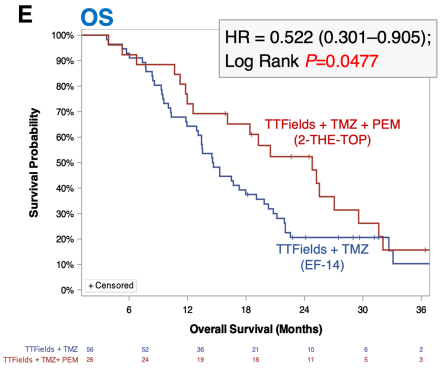

Figure 1. 2-THE-TOP study design and survival endpoints

(A) Top: the 2-THE-TOP study assessed the efficacy of adjuvant TTFields combined with pembrolizumab and TMZ in newly diagnosed GBM patients, following standard chemoradiation. Patients began TTFields therapy with cycle 1 of TMZ, with pembrolizumab added in cycle 2. Tumor and PBMC samples were collected at designated time points for correlative analyses. Bottom: the study objectives. Patients were stratified by MGMT promoter methylation status and extent of resection (maximal resection vs. biopsy only).

(B) A CONSORT flowchart detailing recruitment and enrollments.

(C) Summary of primary and secondary survival endpoints.

(D) The median PFS from enrollment was 12 months for the 26-patient PP group, compared to 5.8 months for the 56-patient case-matched control cohort treated with TTFields plus TMZ from the experimental arm of the EF-14 study (HR 0.377; 95% CI 0.217–0.653; log rank $p = 0.00261$).

(E) The median OS from enrollment was 24.8 months for the PP population, compared to 14.6 months for case-matched controls (HR 0.522; 95% CI 0.301–0.905; log rank $p = 0.0477$).

comprised 31 patients, with the per-protocol (PP) group of 26 and 28 patients evaluable for safety (Tables S1 and S2). In the ITT and PP populations, the median ages were 60.7 and 60.5 years, with 71% and 73% men, respectively, 29% and 27% were biopsy only, 68% and 73% had an unmethylated O-6-methylguanine-DNA methyltransferase (MGMT) promoter, and 13% and 12% had an isocitrate dehydrogenase 1 (IDH1) or IDH2 mutation—assessed by IHC and DNA sequencing. PBMC and tumor samples collected and available for correlative analysis are detailed in Table S3.

Because the PP population was enriched in adverse prognostic factors compared to the general EF-14 study (e.g., higher rates of male sex, unmethylated MGMT, biopsy only), we created a case-matched control cohort of 56 patients from the EF-14 trial (TTFields plus TMZ) with similar key characteristics, including median age, sex, KPS, extent of resection, MGMT promoter methylation, IDH mutation status, and TTFields usage during the first 6 months (Table S1, and see STAR Methods for details on cohort creation). During accrual, updates to the World Health Organization classification excluded IDH1/2 mutant tumors from GBM[22]; thus, for the last 8 enrollments, only wild-type IDH (WT-IDH) GBM were included, and no patients enrolled after this point met the GBM criteria only based on this new classification (e.g., tumors previously described as molecular GBM[23,24]). In this WT-IDH GBM subset (23 patients), the median age was 60.8 years, 74% were males, 30% were biopsy only, and 74% had an unmethylated MGMT promoter (Table S1).

Safety

Throughout the pilot trial, we meticulously monitored and documented all the adverse events. Of the 695 recorded events, 213 (31%) were investigational treatment related, with only 16 events (7.5% of treatment-related events) classified as Common Terminology Criteria for Adverse Events grade 3 or higher. The toxicity table (Table S4) offers a comprehensive overview of these 213 potential treatment-related toxicity events. The most common events were dermatological (notably scalp irritation from TTFields array placement) and gastrointestinal (primarily mild to moderate nausea likely linked to TMZ and pembrolizumab). Overall, the triple regimen (TTFields + TMZ + pembrolizumab) exhibited a manageable safety profile with few severe events, supporting further clinical development.

Please cite this article in press as: Chen et al., Efficacy and safety of adjuvant TTFields plus pembrolizumab and temozolomide in newly diagnosed glioblastoma: A phase 2 study, Med (2025), https://doi.org/10.1016/j.medj.2025.100708

TTFields plus pembrolizumab and TMZ is associated with extended survival

At data cutoff, 5 patients had not progressed and 7 remained alive. In the ITT and PP populations, including patients with IDH1/2 mutant tumors, median PFS was 11.9 months (95% confidence interval [CI] 8.83–16.6) and 12.0 months (95% CI 8.83–21.1), respectively, while median OS was 22.1 months (95% CI 13.9–27) and 24.8 months (95% CI 12.57–29.57). Among 23 WT-IDH GBM patients, median PFS and OS were 10.8 months (95% CI 7.4–16.6) and 20.5 months (95% CI 12.5–25.5), respectively (Figure 1C). Compared to a 56-patient case-matched control cohort from the EF-14 study, the PP population demonstrated significantly longer median PFS (12 vs. 5.8 months; hazard ratio [HR] 0.377; 95% CI 0.217–0.653; log rank p = 0.00261) and OS (24.8 vs. 14.6 months; HR 0.522; 95% CI 0.301–0.905; log rank p = 0.0477) (Figures 1D and 1E).

TTFields were linked to survival and adaptive immunity via a T1IFN trajectory in DCs

TTFields were recently shown to induce intratumoral immune activation via cGAS/STING and AIM2/caspase-1-dependent inflammasomes, leading to systemic adaptive immunity through a T1IFN pathway in DCs.[19] To validate this mechanism in a larger cohort and link it to treatment response and survival, we collected paired 5′ scRNA-seq and TCRα/β V(D)J sequencing data from serial PBMC samples starting at the Pre-TTF time point (Figure 1A). We used Seurat for graph-based clustering,[25,26] uniform manifold approximation and projection (UMAP) for dimensionality reduction,[27] and Simpson's diversity index to assess TCR clonotype diversity,[28] and compared TCRβ clonotypes of primary and recurrent (where available) tumors with corresponding PBMCs to track T cell clonal evolution. Of the 26 PP patients, 21 had complete serial blood collections, contributing a total of 102 PBMC samples (16 maximal resection, including 14 WT-IDH tumors, and 5 biopsy-only tumors, all WT-IDH). The other 5 (3 maximal resection and 2 biopsy only) were excluded due to unusual sequence output from the first 2 treatment time points (Table S3). In total, 576,406 single PBMCs were resolved into 22 immunologically defined cell types, annotated as described earlier[19] (Figure 2A).

Consistent with its complete *in situ* immunization platform via DNA sensor inflammasomes,[17–19] TTFields treatment was specifically associated with increased expression of the 99-gene T1IFN pathway (GO: 0034340) in DCs—but not the 73-gene non-T1IFN inflammatory pathway (GO: 002437)—shortly after TTFields initiation (Pre-TTF to C1, before pembrolizumab, compared to C1–C2; Figures 2B and 2C). In a multivariable Cox proportional hazards model (Cox PH), accounting for key prognostic factors and survival for both the PP and WT-IDH GBM populations, T1IFN pathway intensity in DCs—but not in the 2 other T1IFN-responsive immune cell types, monocytes and natural killer (NK) cells—emerged as a strong predictor of survival (HR 0.27 and 0.31; p = 0.024 and 0.034 for PP and WT-IDH GBM populations, respectively; Figure 2D), whereas non-T1IFN pathway expression in DCs did not correlate with outcomes (Figure 2D). Given that T1IFN is an innate immune signal with rapid kinetics, the 2.5-month gap between the start of chemoradiation and the Pre-TTF time point suggests that the observed T1IFN response is primarily driven by TTFields, with any residual effects from chemoradiation likely playing only a minor role.

From DCs, the T1IFN pathway engaged the adaptive immune system, showing a strong correlation with the 556-gene T cell activation pathway (GO: 0042110) in T cells by C4 pembrolizumab (Pearson r = 0.81; p = 0.000027) (Figure 2E), which in turn predicted survival (HR 0.44 and 0.07, p = 0.035 and 0.039 for PP and WT-IDH GBM populations, respectively) in the same Cox PH model (Figure 2F). Consistent with previous findings,[19] T cell clonal expansion—measured by the Simpson's diversity index of TCRB clonotypes—was observed from Pre-TTF to Post-TTF (prior to C1 pembrolizumab) but not after pembrolizumab initiation (C1–C4) (Figures 3A and S1), suggesting that while the initial immune activation by TTFields was crucial, sustained anti-tumor immunity may require additional effects from pembrolizumab.

TCR clonal replacement is crucial for immune adaptation to neoantigen variations in the TME, particularly in the context of ICI.[29,30] We hypothesized that continuous TTFields application drives the expansion of new TCR clones targeting emerging tumor-associated antigens, potentially at the expense of previously dominant clones, a process that may be enhanced by pembrolizumab. TCR clonal replacement is measured as the ratio of the prevalence of dominant clones at a given time to that of the previously dominant clones that were supplanted. Tracking the top 10 and 20 TCRβ clones across all PP patients revealed significant clonal replacement between Pre-TTF and C4, both before and after pembrolizumab (Figures 3B, 3C, and S2), demonstrating the sustained intratumor immunizing effect of continuous TTFields.

In a univariate analysis, when replacement ratios were dichotomized around the mean for each period, only a high replacement ratio from C1 to C4 predicted extended survival, while ratios for Pre-TTF to C1 and Pre-TTF to C4 did not (Figure 3D); similar results were observed with the top 20 clonal replacement (Figure S3). Thus, while TTFields appears to drive T cell clonal expansion from Pre-TTF to Post-TTF (C1), pembrolizumab was associated with selective expansion of these TTFields-induced clones during the C1–C4 interval. Indeed, a strong correlation between C1–C4 clonal replacement and T cell activation (Pearson r = 0.72; p = 0.0018; Figure 3E) supports that this selective expansion is a key factor in improved survival. Although we cannot completely dismiss a delayed TTFields effect on selective T cell expansion, this is less likely given that a high replacement ratio from Pre-TTF to C4, which spans both pre- and post-pembrolizumab periods, did not predict extended survival (Figure 3D).

In summary, local TTFields therapy initiates an antigen-specific adaptive immune response in the periphery via the T1IFN trajectory in DCs, which is selectively amplified by anti-PD-1 immunotherapy, highlighting their potential synergistic *in situ* immunizing effects.

Patients with biopsy tumors exhibited longer survival than those with maximal resection

To explore the synergistic immunizing effects of TTFields and pembrolizumab, we hypothesized that larger tumor burdens, such as

Please cite this article in press as: Chen et al., Efficacy and safety of adjuvant TTFields plus pembrolizumab and temozolomide in newly diagnosed glioblastoma: A phase 2 study, Med (2025), https://doi.org/10.1016/j.medj.2025.100708

CellPress
OPEN ACCESS

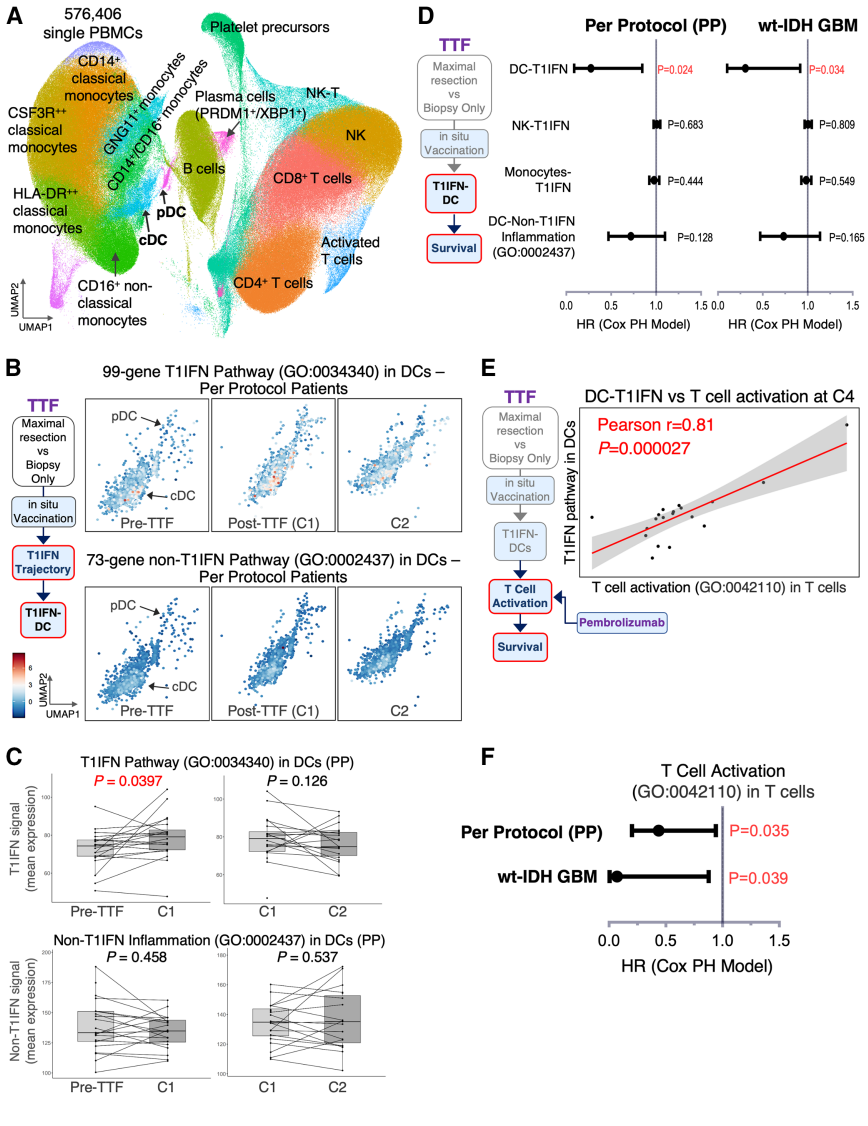

Figure 2. TTFields-mediated T1IFN pathway induction in DCs is associated with T cell activation and serves as a prognostic indicator of survival

(A) Two-dimensional (2D) UMAP (resolution 1) of 576,406 single PBMCs in 102 blood samples across 21 patients, highlighting 22 immune cell subtypes. cDC, conventional DCs; pDC, plasmacytoid DCs; NK, natural killer cells; NK-T, NK T cells.

(B and C) T1IFN pathway activation in DCs induced by TTFields treatment. (B) Left: stepwise model illustrating intratumor immunization by TTFields via the T1IFN pathway in DCs. Right: 2D UMAP of single DCs displaying mean expression of the T1IFN (top) and non-T1IFN inflammatory (bottom) pathways at indicated treatment times in all PP patients. (C) Combination box and whisker and dot plots depicting the mean expression of T1IFN (top) and non-T1IFN (bottom) signals in DCs at the indicated treatment periods (Pre-TTF to Post-TTF or C1 and C1–C2), demonstrating a significant increase in T1IFN, but not in non-T1IFN, signals in DCs immediately following TTFields treatment (Pre-TTF to C1), with no significant changes observed after pembrolizumab (C1–C2). Data are represented as mean ± SEM. The whiskers are the minimum and maximum values, the lower and upper box edges are the 25th and 75th percentage values, respectively, and the lines within the boxes are the median. N = 21. Comparisons were performed using the Wilcoxon test.

(D) Left: stepwise model illustrating intratumor immunization by TTFields via the T1IFN pathway in DCs, leading to improved survival. Right: line graphs displaying HR with 95% CI from a multivariate Cox PH model incorporating the T1IFN pathway in DCs (DC-T1IFN), NK, and monocytes or the non-T1IFN inflammatory pathway in DCs in the PP (N = 21) and WT-IDH GBM-only populations (N = 19). Comparisons were performed using the Wald test in R.

(E) Left: stepwise model of intratumor immunization by TTFields via the T1IFN-DC pathway to T cells and survival. Right: scatterplot showing the correlation between DC-T1IFN signals at Post-TTF (C1) and the T cell activation pathway in T cells at C4 pembrolizumab, demonstrating a strong Pearson correlation (r = 0.81; p = 0.000027). N = 19.

(F) Line graphs illustrating HR with 95% CI derived from a multivariate Cox PH model, incorporating the T cell activation pathway in T cells at C4 pembrolizumab in the PP (N = 19) and WT-IDH GBM only (N = 17) populations. Comparisons were performed using the Wald test in R.

those in biopsy-only patients, would elicit stronger anti-tumor immunity detectable in PBMCs, thereby improving response and survival compared to maximal resection. We compared survival outcomes between these groups in the 2-THE-TOP study and 56 matched controls. Notably, biopsy-only patients showed markedly greater improvements in PFS and OS relative to controls, whereas maximal resection patients showed only modest gains (Figure 4A). Within the 2-THE-TOP cohort, 7 biopsy-only WT-IDH GBM patients were compared to 23 WT-IDH patients who underwent maximal resection, with both groups having similar clinical and molecular profiles (Figure 4B). Representative patients with maximal resection and biopsy-only WT-IDH tumors are shown with their treatment timelines, steroid exposure, and serial brain MRI in Figure 4C. Best responses, defined as percent change of measurable tumors from baseline per iRANO criteria,[21] showed that among the 7 biopsy-only patients, 2 achieved a durable complete/near-complete response, 2 reached a partial response, 2 maintained durable stable disease, and 1 initially exhibited tumor reduction before succumbing to complications following seizures (Figure 4D). As predicted, the biopsy-only group had significantly improved outcomes, with median PFS of 27.2 vs. 9.6 months (HR 0.37; 95% CI 0.16–0.85; log rank p = 0.014) and median OS of 31.6 vs. 18.8 months (HR 0.4; 95% CI 0.17–0.92; log rank p = 0.023) (Figures 4E and 4F). Although the markedly higher survival and response rates in biopsy-only patients were unexpected, given the historical association of biopsy-only GBM with poor outcomes under standard chemoradiation,[2–4] these findings align with our prior studies demonstrating TTFields as an effective *in*

Please cite this article in press as: Chen et al., Efficacy and safety of adjuvant TTFields plus pembrolizumab and temozolomide in newly diagnosed glioblastoma: A phase 2 study, Med (2025), https://doi.org/10.1016/j.medj.2025.100708

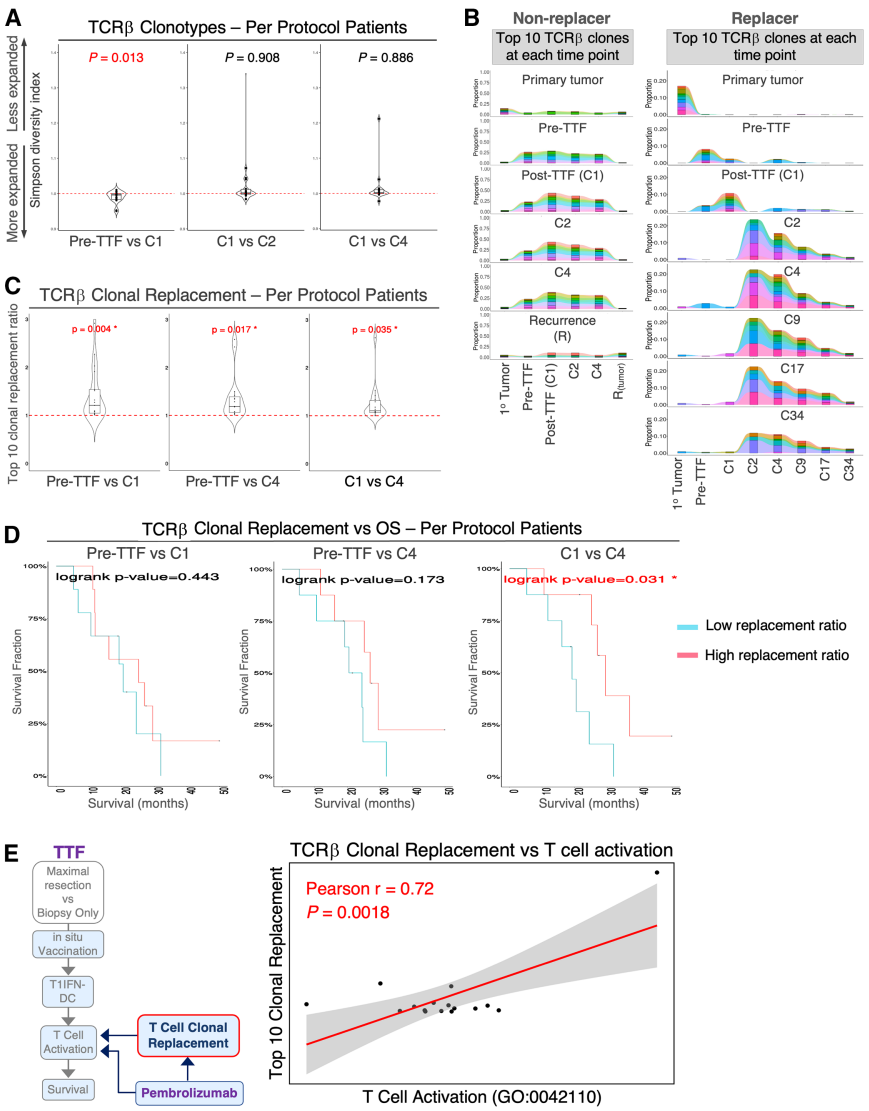

Figure 3. The TCR clonal replacement ratio following pembrolizumab therapy predicts patient survival

(A) Combination violin, box and whisker, and dot plots illustrating TCRβ clonal diversity, calculated using the Simpson diversity index, across different treatment periods in the PP population, confirming significant TCR clonal expansion associated with TTFields treatment, whereas pembrolizumab administration did not induce TCR clonal expansion. *N* = 19.

(B) Tracking the top 10 most expanded TCRβ clones at each treatment time point in PP patients. Representative examples illustrate patients with high (Replacer) vs. low (Non-replacer) TCRβ clonal replacement by C4 pembrolizumab.

(C) Combination violin, box and whisker, and dot plots illustrating the top 10 TCRβ clonal replacement ratios during indicated treatment periods in PP patients, demonstrating that TCRβ clonal replacement occurs consistently following both TTFields and pembrolizumab treatments. Clonal replacement ratio is defined as the prevalence of the top 10 dominant TCR clones at a specific time point relative to that of previously dominant, supplanted clones. *N* = 19.

(D) TCRβ clonal replacement ratio between C1 and C4 of pembrolizumab predicts extended survival: Kaplan-Meier survival plots stratify patients into low and high top 10 TCRβ clonal replacement ratio groups based on the median for each treatment period. A high top 10 TCRβ clonal replacement ratio between C1 and C4 pembrolizumab was significantly associated with extended survival. *N* = 19.

(E) Left: stepwise model of *in situ* immunization by TTFields via the DC-T1IFN pathway, promoting T cell activation and survival, with contributions from pembrolizumab and TCR clonal replacement. Right: scatterplot of the top 10 TCRβ clonal replacement ratios (C1–C4) vs. the T cell activation pathway in T cells at C4 pembrolizumab, showing a strong Pearson correlation ($r = 0.72$; $p = 0.0018$). *N* = 19. Data are represented as mean ± SEM. The whiskers are the minimum and maximum values, the lower and upper box edges are the 25th and 75th percentage values, respectively, and the lines within the boxes are the median. Comparisons were performed using paired Student's t test with a 2-tailed distribution for (A) and (C), and log rank test for (D).

situ immunizing platform for GBM.[19] We suggest that the presence of a large residual tumor mass in biopsy-only cases provides sufficient antigen load to drive robust anti-tumor immunity, although the potential contribution of prior chemoradiation cannot be entirely excluded.

Pre-treatment characteristics of primary tumors and peripheral T cells in maximal resection versus biopsy-only patients

To determine whether the survival advantage in biopsy-only patients was due to TME differences rather than treatment effects, we analyzed all available primary WT-IDH tumors—14 from maximal resection and 6 from biopsy-only cases—for variations in tumor mutational burden (TMB) using WES, as TMB correlates with ICI response in many solid tumors.[31] Our analysis revealed no significant differences in functional TMB, stop-gain SNPs, or in/del mutations between the groups, although maximal resection tumors showed a slight increase in stop-loss SNP (Figure S4A). Additionally, clinical genomics reports, including data from all 7 biopsy-only tumors, showed no notable differences in the frequency of mutations, deletions, or amplifications in key GBM prognostic genes (e.g., *CDKN2A/B*, *EGFR*, *RB1*, *TP53*, *PTEN*[32]) or in genes involved in DNA excision repair and microsatellite stability (e.g., *MLH1*, *MSH2*, *POLE*[33]) (Figure S4B).

Next, we analyzed primary WT-IDH GBM tumors available for bulk RNA-seq—after depleting 2 samples per group during TMB analysis, 12 maximal resection and 4 biopsy-only cases remained. Our analysis revealed upregulation of GO pathways involved in MDSC recruitment, activation, and retention (e.g., negative chemotaxis, monocyte activation, and interleukin-9

Please cite this article in press as: Chen et al., Efficacy and safety of adjuvant TTFields plus pembrolizumab and temozolomide in newly diagnosed glioblastoma: A phase 2 study, Med (2025), https://doi.org/10.1016/j.medj.2025.100708

A

Maximal Resection vs. Biopsy Only in 2-THE-TOP Per Protocol vs Matched 56

Study Population	Max Resection (%)	Biopsy (%)	pMGMT (%)	TTF Usage (mean)	mPFS [mo]	HR (95% CI)	*log rank P*	mOS [mo]	HR (95% CI)	*log rank P*
Biopsy Only–2THETOP	0	100	29	85	27.2	0.15 (0.04–0.63)	*0.025*	31.6	0.16 (0.04–0.75)	*0.05*
Biopsy Only–Matched56	0	100	20	81	7			13.5		
Max Resection–2THETOP	100	0	19	79	10.8	0.4 (0.21–0.75)	*0.03*	24.8	0.65 (0.34–1.24)	*0.25*
Max Resection–Matched56	100	0	20	76	5.1			15.3		

B

Max Resection vs. Biopsy Only (2-THE-TOP)

N patients (23)	Max Resection	Biopsy Only
Age, median(range)	62(34-79)	60(31-69)
Male sex (%)	12(75)	5(71)
KPS, %, median(range)	80(70-90)	80(80)
Unmethylated MGMT, %	75	71
Dexa, mg, median(range)	0(0-4)	1(0-3)
TMZ, Median(range)	7 (2-12)	12 (2-12)
TTF usage, %(range)	78(55-95)	85(75-91)
Pembro, median(range)	9(1-9)	9(4-9)

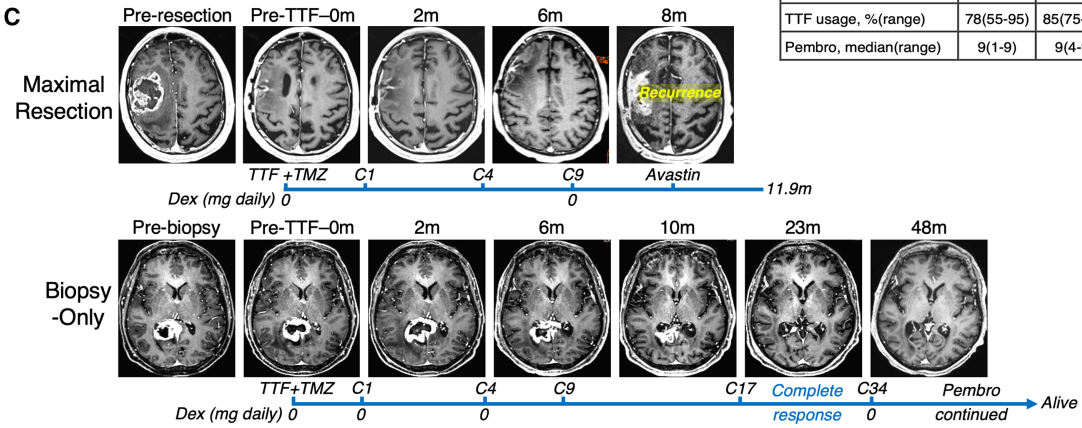

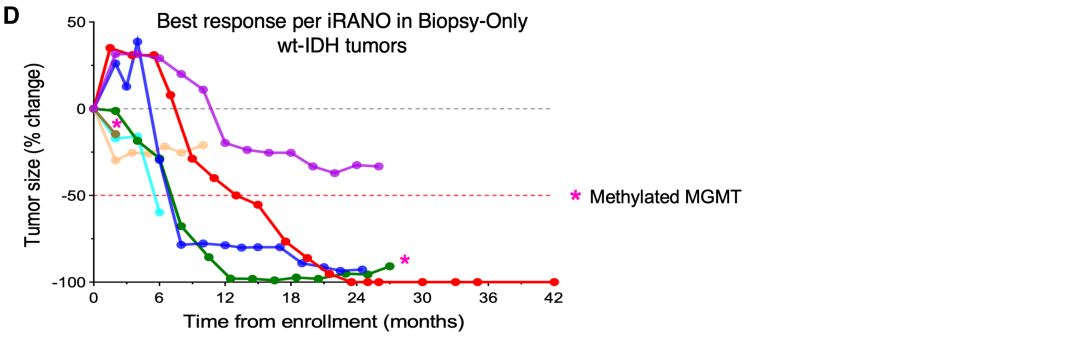

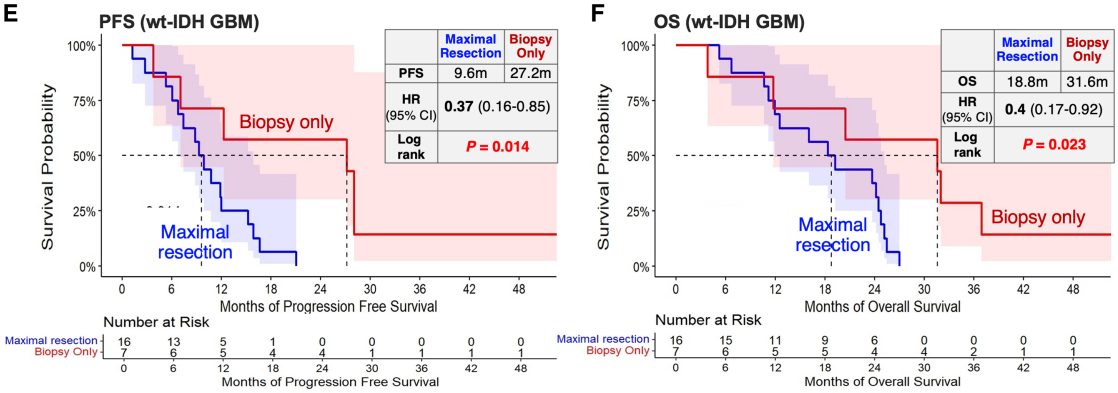

Figure 4. Patients with biopsy-only WT-IDH GBM exhibit longer survival compared to those with maximal resection

(A) Summary of survival in maximal resection and biopsy-only patients in 2-THE-TOP as compared to the case-matched control.

(B) Patient characteristics for maximal resection and biopsy-only groups within the 2-THE-TOP WT-IDH GBM cohort.

(C) Representative serial brain MR images and treatment timelines for a patient with a maximal resection WT-IDH tumor (top), showing early progression, and a patient with a biopsy-only WT-IDH tumor (bottom), demonstrating a complete response.

(D) Line graph showing the best tumor responses in biopsy-only WT-IDH GBM patients, measured as percentage changes in tumor size relative to baseline Pre-TTF tumor size. Tumor size was calculated as the sum of the products of 2 perpendicular dimensions of all target lesions.

(legend continued on next page)

[*IL-9*], *IL-21*, and *IL-23* signaling), as well as pathways related to hypoxic responses and neuronal activities in GBM and glioma stem-like cells[34,35] (Figure S4C). In a multivariable Cox PH model, high expression of these pathways correlated with poorer outcomes, whereas TIL markers (TCR complex and $CD4^+$ and $CD8^+$ differentiation) correlated with improved survival, although the functional pathways associated with these TILs did not reflect the survival benefit. This is consistent with evidence that GBM TILs are largely dysfunctional[36,37] and contribute to tumor-promoting activities rather than antitumor responses. Notably, key innate immune pathways bridging the innate and adaptive immune systems, those involving DC differentiation (HR 0.006; 95% CI 0–0.167; $p = 0.0026$) and positive regulation of microglial migration (HR 0.003; 95% CI 0–0.114; $p = 0.0017$), were strongly linked to improved survival (Figure S4C). Importantly, no differences in these pathways were observed between maximal resection and biopsy-only tumors (Figure S4D), supporting our hypothesis that bulky, biopsy-only tumors provide an ideal setting for TTFields plus pembrolizumab to engage the innate immune system and promote intratumor immunization, an effect likely diminished following maximal tumor resection.

Lastly, to determine whether patients with biopsy-only WT-IDH tumors exhibit inherently more robust T cell activity before treatment than those with maximal resection, we isolated T cells from PBMCs in both groups via $CD3^-$ selection for bulk RNA-seq analysis. Employing GeneRep/nSCORE, a validated gene network-based algorithm with an automated 3-dimensional (3D) visualization pipeline,[38] we mapped master regulatory hubs governing T cell biology at the Pre-TTF time point (immediately before adjuvant TTFields and TMZ) and at subsequent study intervals. At Pre-TTF, the immune regulatory hub (hub 1.1) in T cells was significantly downregulated in biopsy-only patients relative to those with maximal resection (Figure S4E), indicating that T cells in biopsy-only patients were more repressed 4 weeks after completing standard chemoradiation (i.e., 2.5 months from the start of chemoradiation). Notably, only after initiating study treatment did hub 1.1 increase specifically in biopsy-only patients compared to the maximal resection group (Figure S4F). These findings suggest that prior chemoradiation may exert an immunosuppressive effect in the presence of large GBM tumors, as previously reported,[39] and that the subsequent increase in T cell activation in biopsy-only patients likely results from the combined effects of TTFields and pembrolizumab, although lingering delayed effects from chemoradiation cannot be entirely excluded.

Biopsy-only WT-IDH tumors were linked to higher adaptive immune activation through the T1IFN trajectory

Assuming TTFields induce cGAS/STING and AIM2/caspase-1-dependent *in situ* immunizing effects, they are expected to promote stronger T1IFN-mediated immune activation in the DC compartment of biopsy-only patients compared to those undergoing maximal resection. As anticipated, T1IFN pathway expression was significantly higher after 4 weeks of TTFields in biopsy-only patients (Pre-TTF to Post-TTF or C1; Figures 5A and 5C). However, following pembrolizumab addition, T1IFN expression in DCs did not differ significantly between the groups, and non-T1IFN pathway expression remained comparable at all time points (Pre-TTF to C2; Figures 5B and 5D). These findings suggest that TTFields specifically enhance T1IFN-mediated immune activation in biopsy-only tumors, potentially countering the severe systemic immunosuppression associated with large GBM tumors.

To delineate differences in T cell evolution between maximal resection and biopsy-only WT-IDH tumors, we evaluated dynamic changes in T cell clusters, their activation pathways, and TCRβ clonal expansion throughout treatment. We isolated 166,391 T cells from PBMCs based on CD3 expression and annotated them using a comprehensive T cell gene set (Figure S5; full list in STAR Methods) as previously described[19] (Figure 6A). Representative T cell tracking for patients with maximal resection and biopsy-only tumors is shown in Figures 6B and 6C, respectively. In biopsy-only patients, the compartments for effector $CD8^+$ (purple arrow) and activated $CD4^+$ T cells (green arrow) were largely empty at the Pre-TTF time point, unlike in maximal resection patients, where these compartments were populated with activated cell (Figures 6A–6C). This aligns with our global expression analyses indicating reduced peripheral T cell activity in biopsy-only patients before TTFields treatment. Activated $CD4^+$ and $CD8^+$ T cells began to populate these compartments only after study treatment initiation in biopsy-only patients. Among the 19 WT-IDH patients with available single T cell data, TCRβ clonal expansion was observed in both patient groups prior to pembrolizumab treatment (Pre-TTF to C1 compared to C1–C2 and C1–C4) but more pronounced in biopsy-only patients (Figures 6D and S6A). Throughout treatment, biopsy-only patients exhibited significantly higher activation of both the T cell activation and the 761-gene adaptive immune response (GO: 0002250) pathways (Figure 6E), leading to substantially greater peaks in central memory (CM) $CD8^+$ and $CD4^+$ T cell numbers, expressed as fold increases over the Pre-TTF baseline, compared to maximal resection patients (Figures 6A–6C, red arrow and asterisk; Figure 6F). Additionally, CM fractions increased later in the treatment course and persisted longer in biopsy-only patients (Figures S6B and S6C).

In summary, local TTFields therapy of GBM initiates an antigen-specific adaptive immune response that is further enhanced by systemic anti-PD-1 immunotherapy, particularly in patients with biopsy-only tumors, demonstrating their potential synergistic *in situ* immunizing effects.

Recurrent tumors exhibited increased expression of alternative immune checkpoints

Next, we examined TME changes between recurrent and primary tumors that might undermine tumor-specific immune

(E) The median PFS from enrollment was 27.2 months for the biopsy-only wt-IDH tumor group in the 2-THE-TOP study, compared to 9.6 months for the maximal resection group (HR 0.37; 95% CI 0.16–0.85; log rank $p = 0.014$).
(F) The median OS from enrollment was 31.6 months for the biopsy-only WT-IDH tumor group in 2-THE-TOP, compared to 18.8 months for the maximal resection group (HR 0.4; 95% CI 0.17–0.92; log rank $p = 0.023$).

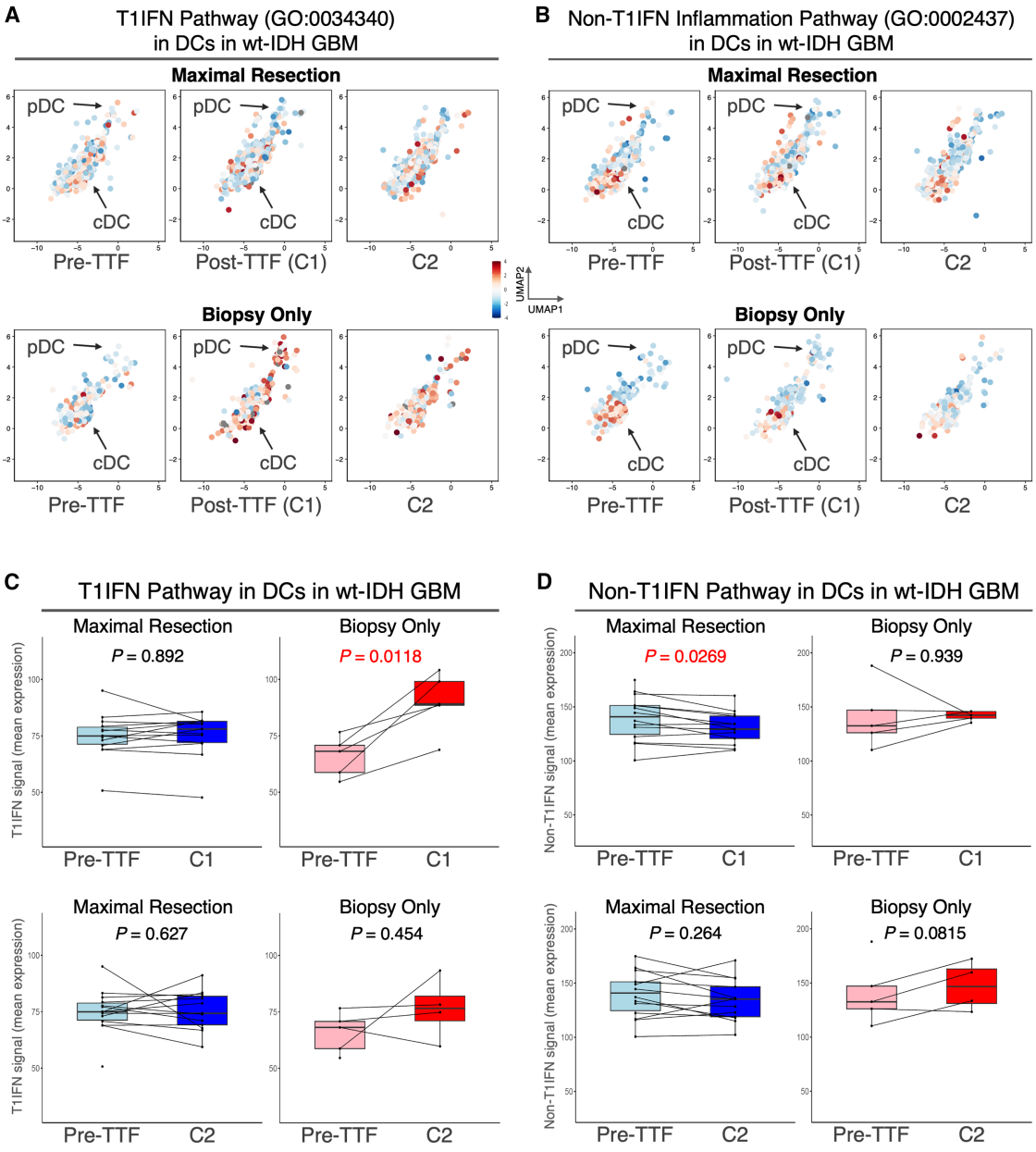

Figure 5. Biopsy-only WT-IDH tumors exhibit more robust T1IFN activation in DCs

(A and B) 2D UMAP plots depicting the mean expression of the T1IFN (A) and non-T1IFN (B) pathways in individual DCs from patients with maximal resection vs. biopsy-only WT-IDH tumors, revealing that biopsy-only patients exhibited significantly higher T1IFN activation in both pDC and cDC populations following TTFields treatment. In contrast, no differences were observed in the expression of the non-T1IFN pathway. *N* = 14, maximal resection; *N* = 5, biopsy-only.

(C and D) Combination box and whisker and dot plots showing relative changes in the mean expression of T1IFN (C) and non-T1IFN (D) signals in DCs across indicated treatment periods in patients with maximal resection and biopsy-only tumors. *N* = 14, maximal resection; *N* = 5, biopsy-only. The data reveal a specific and significant signal increase in T1IFN, but not non-T1IFN, in DCs following TTFields treatment (Pre-TTF to Post-TTF or C1), but not after pembrolizumab was added (Pre-TTF to C2). Data are represented as mean ± SEM. The whiskers are the minimum and maximum values, the lower and upper box edges are the 25th and 75th percentage values, respectively, and the lines within the boxes are the median. Comparisons were performed using the Wilcoxon test.

efficacy and lead to treatment failure. In 9 paired primary and recurrent WT-IDH tumor samples, GeneRep/nSCORE[38] revealed elevated regulatory hubs in recurrent tumors (Figure 7A). Hub 1.1 comprised pathways related to hypoxic response and epithelial-mesenchymal transition (Figures S7A and S7B), which promote glioma stem-like cell (GSC) survival, TME-mediated immunosuppression, and tumor invasion via focal adhesion and cell junction dynamics.[40,41] Hub 1.4 involved cell-cell interactions related to glio-neural development, axonal, and neurotransmitter signaling (Figure S7C) pathways that GSCs may

Please cite this article in press as: Chen et al., Efficacy and safety of adjuvant TTFields plus pembrolizumab and temozolomide in newly diagnosed glioblastoma: A phase 2 study, Med (2025), https://doi.org/10.1016/j.medj.2025.100708

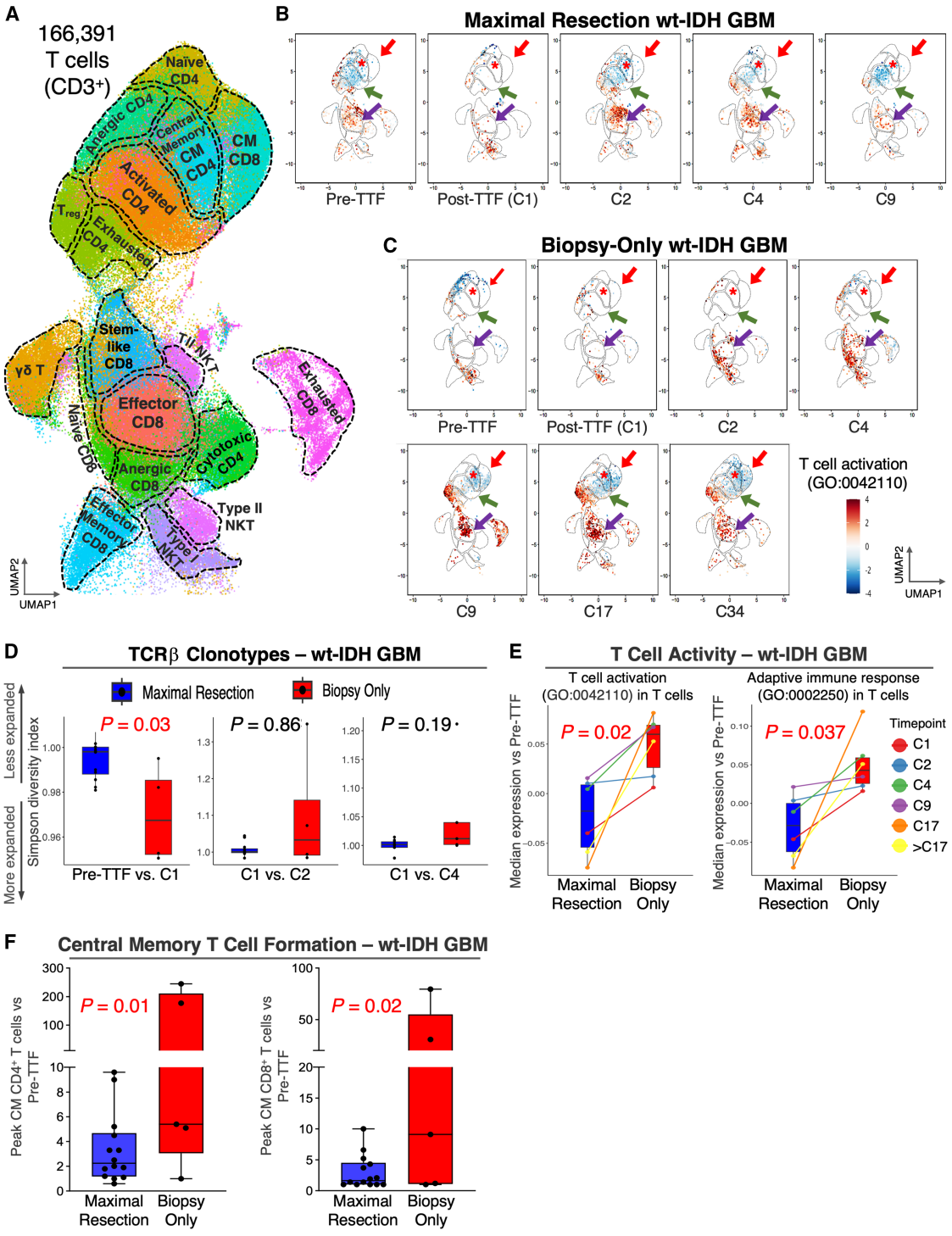

Figure 6. Biopsy-only tumors are associated with higher T cell activation and central memory T cell formation

(A) 2D UMAP plot of all T cells at resolution 1, depicting 18 major CD4$^+$ and CD8$^+$ T cell subtypes.

(B and C) 2D UMAP plots of T cell clusters displaying the activation status of the T cell activation pathway in representative patients with maximal resection (B) or biopsy-only (C) WT-IDH tumors, showing a progressive shift toward activated and central memory (CM) T cell formation in the biopsy-only patient. Purple arrow: effector CD8$^+$ T cells; red arrow: CM CD8$^+$ T cells; green arrow: activated CD4$^+$ T cells; red asterisk: CM CD4$^+$ T cells.

(D) Combination box and whisker and dot plots illustrating TCRβ clonal diversity, measured by the Simpson diversity index, across various treatment periods in patients with maximal resection or biopsy-only WT-IDH GBM tumors. *N* = 14, maximal resection; *N* = 5, biopsy-only.

(legend continued on next page)

Please cite this article in press as: Chen et al., Efficacy and safety of adjuvant TTFields plus pembrolizumab and temozolomide in newly diagnosed glioblastoma: A phase 2 study, Med (2025), https://doi.org/10.1016/j.medj.2025.100708

exploit to enhance survival, invasion, and resistance.[42,43] Finally, Hub 1.7 encompassed mixed immune and inflammatory pathways—some supporting anti-tumor responses (Figure S7D) and others enriched with genes that drive pathological inflammation, recruit suppressive cells, and facilitate immune evasion by GSCs (Figure 7B)—consistent with a recently described mechanism of TTFields resistance in GBM cells.[44]

To further elucidate the interplay between GBM cells and immune evasion mechanisms, we analyzed immune regulatory subnetworks derived from deconvolved immune and non-immune components within the TME of the 9 paired primary and recurrent WT-IDH tumors (Figure 7C). In recurrent GBM, non-immune cells exhibited reactivation of pathways regulated by CEBPB and ATF5, key drivers of GSC maintenance, neural differentiation, metabolism, migration, and immune evasion via checkpoint mechanisms.[45,46] In addition, the senescence and metabolic regulator CREG1 dominated the immune pathway in both compartments, orchestrating various checkpoint mechanisms. This is consistent with the activation of alternative checkpoints pathways following anti-PD-1 therapy, including phosphatidylinositol 3-kinase/AKT/mammalian target of rapamycine[47,48] and tumor necrosis factor-α/nuclear factor κB[49,50] signaling in the immune/inflammatory Hub 1.7 (Figure S7E). Notably, we observed downregulation of the *PD-1/PD-L1* axis, along with decreased expression of indoleamine 2,3-dioxygenase 1 (*IDO1*), lymphocyte-activation gene 3 (*LAG3*), and T-cell immunoglobulin and ITIM domain (*TIGIT*), while alternative checkpoints such as the *TIM-3*/galectin-9 (*LGALS9*) axis, V-domain Ig suppressor of T cell activation (*VISTA* or *VSIR*), *PVR* (poliovirus receptor, a TIGIT ligand), and *CD276* (*B7-H3*) were significantly upregulated in non-immune cells (Figure 7C). These data suggest that selective upregulation of alternative immune checkpoints may contribute to therapeutic resistance.

This pattern of adaptive resistance, marked by elevated alternative immune checkpoints, aligns with ICI resistance observed in other solid tumors.[51,52] In our 9 paired samples, we confirmed the upregulation of *TIM-3/LGALS9*, *VISTA*, *PVR*, and *CD276* (*B7-H3*) at both the mRNA (Figure 7D) and protein (Figure 7E) levels, concurrent with downregulated *PD-1/PD-L1* axis, *TIGIT*, and *LAG3*. Importantly, this immune checkpoint profile was not observed in an RNA-seq dataset from a historical GBM cohort treated with either TMZ alone or TMZ plus TTFields.[53] Additionally, recurrent tumors exhibited increased major histocompatibility complex class I (MHC class I) expression (Figure 7D), suggesting that MHC class I downregulation is not a primary mechanism of immune evasion in these cases.

Collectively, these findings indicate that adjuvant TTFields combined with anti-PD-1 immunotherapy and TMZ is well tolerated and may offer survival benefits, particularly in patients with large, inoperable tumors, by enhancing antigen-specific T cell dynamics and sustaining immune responses. However, the concurrent downregulation of PD-1/PD-L1 and the upregulation of alternative immune checkpoints may underlie resistance mechanisms, leading to tumor relapse.

DISCUSSION

While anti-PD-1 therapies have shown limited efficacy in newly diagnosed GBM,[8,9] the incorporation of pembrolizumab into the adjuvant regimen with TMZ and TTFields in the 2-THE-TOP study yielded encouraging improvements in both PFS and OS, compared to case-matched controls, despite the high prevalence of adverse prognostic factors. Notably, the WT-IDH GBM patients treated with biopsy only—historically an understudied group associated with poor outcomes and representing roughly 25% of cases[2–4,54]—demonstrated significantly better survival than those undergoing maximal resection, aligning with previous findings that TTFields provide greater survival benefits in patients with higher tumor burdens in both newly diagnosed[1] and recurrent[55] settings. These results reinforce the role of TTFields as a complete *in situ* immunization platform: shortly after starting TTFields and TMZ (prior to pembrolizumab), a significant increase in global immune activation along a T1IFN trajectory in DCs promoted enhanced T cell activation, clonal expansion, and survival. Moreover, although T cell clonal replacement began within the first month of TTFields treatment, only the replacement ratio from C1 and C4 pembrolizumab correlated with survival, suggesting that newly expanded T cell clones following TTFields are most critical for improved outcomes.

Lastly, recurrent tumors resistant to the study treatment exhibited an immunosuppressive TME similar to the primary tumors, but with a distinct alternative immune checkpoint profile—most notably, the *TIM-3/LGALS9* axis, *VSIR*, *PVR*, and *CD276* (*B7-H3*). Although these alternative checkpoints have been linked to ICI resistance in other solid tumors,[51,52] our analysis provides detailed insight into TME network alterations, revealing complex changes in key regulatory elements that may promote immune evasion and tumor survival through mechanisms involving immune checkpoints, cellular senescence, and hypoxic pathways in both immune and non-immune TME components.

Limitations of the study

(1) The single-arm design and small sample size, especially within the biopsy-only cohort, limit a definitive evaluation of the triple regimen's efficacy. While major differences in comorbid conditions between the maximal resection

(E) Combination box and whisker and dot plots showing the median expression of T cell activation and adaptive immune response pathways in T cells across treatment time points, normalized to Pre-TTF values, in patients with maximal resection or biopsy-only WT-IDH tumors. *N* = 14, maximal resection; *N* = 5, biopsy-only.

(F) Combination box and whisker and dot plots illustrating the peak fold change in CM $CD4^+$ (left) and $CD8^+$ (right) T cells following study treatment, normalized to Pre-TTF values, in patients with maximal resection vs. biopsy-only WT-IDH tumors. *N* = 14, maximal resection; *N* = 5, biopsy-only. Data are represented as mean ± SEM. The whiskers are the minimum and maximum values, the lower and upper box edges are the 25^{th} and 75^{th} percentage values, respectively, and the lines within the boxes are the median. Comparisons were performed using the paired Student's t test for (D) and (E) and unpaired Student's t test with a 2-tailed distribution for (F).

Please cite this article in press as: Chen et al., Efficacy and safety of adjuvant TTFields plus pembrolizumab and temozolomide in newly diagnosed glioblastoma: A phase 2 study, Med (2025), https://doi.org/10.1016/j.medj.2025.100708

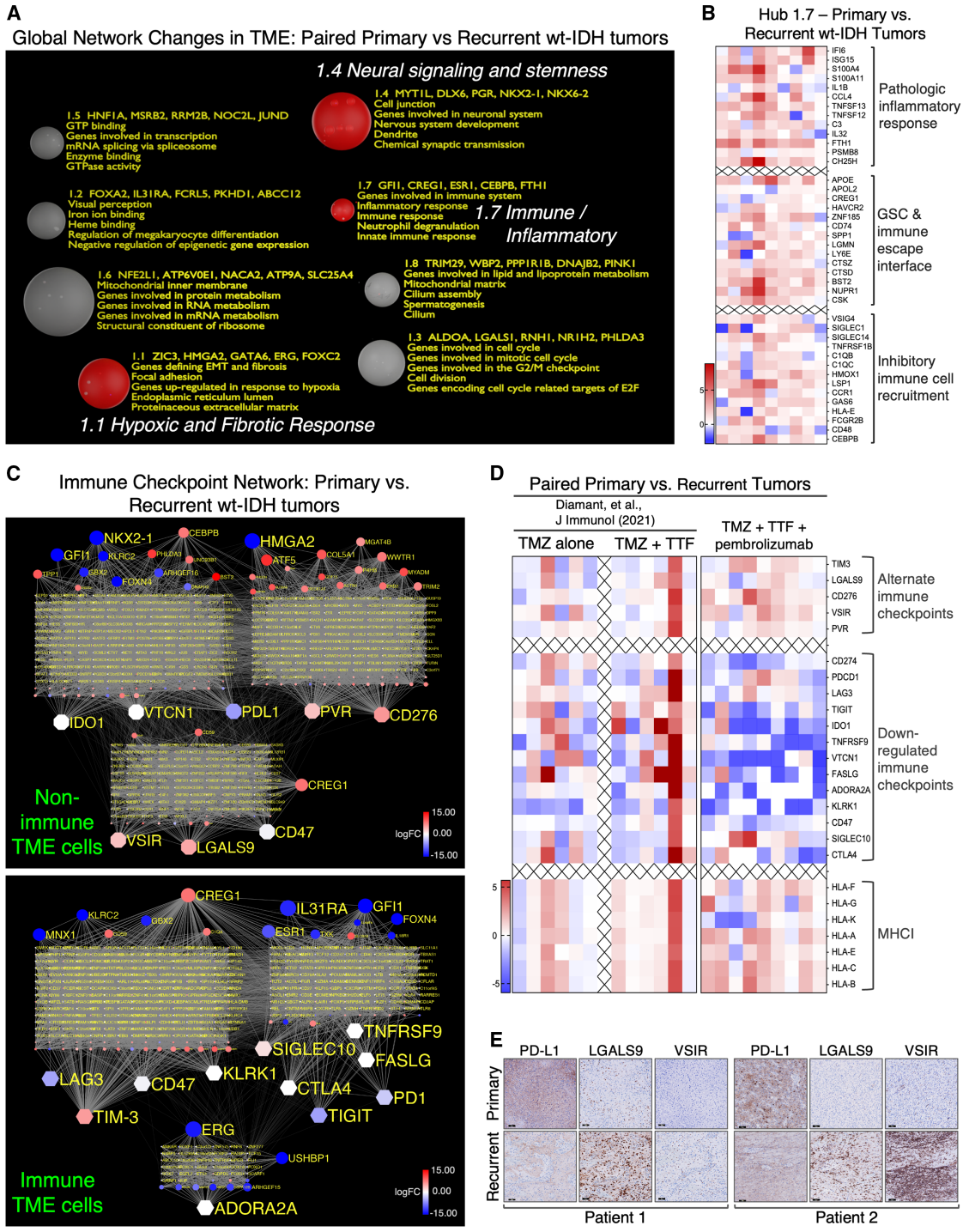

Figure 7. TME reprogramming in recurrent WT-IDH GBM tumors

(A) A 3D map of the activation status of GeneRep/nSCORE-generated global pathway hubs in bulk RNA-seq expression profiling of 9 paired primary vs. recurrent tumor samples in the WT-IDH GBM population. Globe size: the number of pathways in a hub; Globe colors: red, upregulated in recurrent tumors; gray, unchanged between primary and recurrent tumors. Gene names listed after a globe number are master regulators of that hub.

(B) A heatmap of fold change in key markers in the inflammation Hub 1.7 in the 9 paired primary vs. recurrent GBM tumors in (A), showing that Hub 1.7 is enriched in pathologic inflammatory response and immune inhibitory and escape gene clusters.

(C) 2D maps of the GeneRep/nSCORE-generated immune checkpoint regulatory subnetwork changes in the deconvoluted immune ($CD45^+$) and non-immune (tumor cells and $CD45^-$ stromal cells) TME cells from the 9 paired primary vs. recurrent GBM tumors, showing the compensatory downregulation of the *PD-1/PD-L1* axis and the downregulation of *IDO1*, *TIGIT*, and *LAG3*, while other alternative immune checkpoints *TIM-3/LGALS9*, *VSIR*, *PVR*, and *CD276* (*B7-H3*) were

(legend continued on next page)

and biopsy-only groups are unlikely to account for the observed outcomes, we cannot rule out the potential impact of undetected underlying comorbidities. While the reliance on historical data introduces potential biases and confounding factors, the favorable safety profile and encouraging survival outcomes, particularly in patients with bulky, biopsy-only tumors (a historically unexpected finding supported by mechanistic data), justify further investigation in a phase 3 randomized placebo-controlled trial.

(2) Because repeated invasive CNS sampling poses significant risks, we used PBMCs as a surrogate to assess TME immunological changes. Peripheral immune alterations, particularly via the T1IFN pathway, closely mirror TME dynamics in GBM models treated with TTFields and were later confirmed in patients.[19] Although a window-of-opportunity study would offer a more definitive assessment and could be the focus for future efforts, our serial PBMC and tumor analyses provide one of the most comprehensive multi-omics datasets in GBM and solid tumor immunotherapy.

(3) The single-arm design also limits our ability to fully rule out prior chemoradiation as a contributor to the heightened immune activation observed in biopsy-only patients compared to those with maximal resection. However, given that the Pre-TTF time point was at least 2.5 months after the start and 4 weeks after the end of chemoradiation, T cells in biopsy-only patients remained suppressed, likely due to the systemic immunosuppression from bulky tumors.[39] In contrast, rapid innate and adaptive immune activation was evident within 4 and 3 weeks of initiating TTFields and pembrolizumab, respectively. Although some delayed chemoradiation effects may complement the treatment, definitively separating these influences would require a trial comparing adjuvant TMZ with adjuvant TTFields with serial multi-omics analysis. However, omitting TTFields is not standard at our institution or many others.

(4) This study did not directly evaluate the impact of adjuvant TMZ, although we expect its effect on immune phenotypes to be minimal or even potentially exacerbate immunosuppression. Dose-intense TMZ (100 mg/m^2/day for 21 days) has been shown to induce a proliferative rebound after lymphopenia that merely restores pre-chemotherapy T cell metrics,[56–58] whereas standard-dose TMZ (150–200 mg/m^2/day for 5 days) used in this study is known for persistent immunosuppressive effects such as lymphopenia and T cell exhaustion.[59,60] In contrast, the selective T1IFN pathway activation in DCs and subsequent T cell activation observed in our study, along with preclinical evidence that TMZ does not significantly interfere with TTFields-induced immune activation,[19] suggest that TMZ's impact is unlikely to confound our findings. Nonetheless, future studies enrolling only MGMT promoter-unmethylated GBM patients could exclude adjuvant TMZ to eliminate this potential confounder.

In summary, these limitations underscore the need for further investigation, ideally in a randomized placebo-controlled trial, to validate the promising survival outcomes, peripheral immune activation, and favorable safety profile of integrating TTFields with anti-PD-1 immunotherapy in newly diagnosed GBM patients.

RESOURCE AVAILABILITY

Lead contact

Requests for further information and resources should be directed to and will be fulfilled by the lead contact, David D. Tran (david.tran@med.usc.edu).

Materials availability

This study did not generate new unique reagents.

Data and code availability

The RNA-seq and DNA-seq data generated in this study with associated clinical metadata have been deposited in Gene Expression Omnibus (GEO) at the following accession numbers: GSE269869, GSE269956, and GSE269957.

The GeneRep-nSCORE algorithm code used in this study to generate global regulatory gene networks can be accessed in GitHub at https://github.com/TranLabUSC/NETZEN-classic. All other bioinformatics codes are described in the STAR Methods and can be accessed at https://github.com/TranLabUSC/2TT_clinical_trial_paper.

Any additional information required to reanalyze the data reported in this paper, as well as the study protocol and statistical analysis plan, are available from the lead contact upon request.

ACKNOWLEDGMENTS

This work was supported in part by research grants from Novocure GmbH to D.D.T. and by the NIH, United States (K08NS099484) to M.R. We would like to thank Gitit Lavy-Shahaf for creating the control cohort from the EF-14 study; Ilan Volovitz for his generous gift of the TMZ alone and TMZ+TTFields RNA-seq dataset; members of the Tran laboratory for their insightful feedback and assistance; Moshe Giladi, Uri Weinberg, Leonardo Lustgarten, Elena Palmesino, Adi Haber, Tali Voloshin Sela, Cathy Chang, and Yiftah Barsheshet for their insightful feedback; and Sonisha Warren, Deborah Sampson, Valerie Greene Layton, Annie Allen, Victoria Hope, Kristine Wynne, Renee Boyette, Ciara Anderson, and Sandra Oviedo for study coordination and regulatory support. We would like to acknowledge the regulatory and technical support of the UF Cancer Center, the Norris Comprehensive Cancer Center (NCCC) of USC Keck Medicine, and the Translational Pathology Core of the NCCC.

upregulated. Shape size: importance rank of a gene. Shape colors: red, upregulated in recurrent tumors; blue, downregulated in recurrent tumors; gray, unchanged between primary and recurrent tumors.

(D) Heatmaps of fold change in the expression of major immune checkpoints and MHC class I molecules in the 9 paired primary vs. recurrent GBM tumors confirmed the predicted downregulation of the *PD-1*/*PD-L1* axis, *TIGIT*, and *LAG3* and the upregulation of the alternative immune checkpoints *TIM-3*/*LGALS9*, *VSIR*, *PVR*, and *CD276* (*B7-H3*). This pattern was not observed in a historical dataset of 12 paired primary vs. recurrent GBM tumors treated with TMZ alone or TMZ plus TTFields.

(E) Representative images of IHC for PD-L1, LGALS9, and VSIR in 2 sets of paired primary vs. recurrent tumors in the 2-THE-TOP study. Scale bar, 50 μm.

AUTHOR CONTRIBUTIONS

All authors have made sufficient contributions to the conception, design, execution, and interpretation of the research study to take public responsibility for appropriate portions of the content. D.C., S.B.L., A.P.G., and D.D.T. had unrestricted access to all data. All authors agreed to submit the manuscript, read, and approved the final draft, and take full responsibility for its content, including the accuracy of the data and the fidelity of the trial to the registered protocol and its statistical analysis. Specific contributions of each author are as follows: S.B.L. led the technical aspects of the multi-omics analysis, designed and implemented non-standard analytical pipelines specifically customized for this project, which were critical in identifying the mechanism central to the manuscript's correlative findings, interpreted the correlative results, and wrote the manuscript. D.C. prepared and processed all multi-omics samples, annotated scRNA-seq clusters, analyzed the mutational data, defined alternative immune checkpoints in recurrent tumors, interpreted the results, and wrote the manuscript. His previous work was critical to the mechanistic interpretation of the correlative work. A.P.G. conducted the clinical study, interpreted the clinical results, and wrote the manuscript. H.M. implemented the customized analytical pipelines and performed the multi-omics data processing and analysis. M.L. performed the statistical analysis of the clinical data and wrote the statistical section. A.O. provided technical assistance in sample processing, data collection, and analysis. M.R. provided clinical expertise and feedback and participated in the clinical trial. D.D.T. conceived the concept of the study, wrote the protocol, secured the funding, conducted the clinical trial, interpreted the results, and wrote the manuscript.

DECLARATION OF INTERESTS

D.D.T. has received research grants from Novocure to support parts of the work and has received personal honoraria from Novocure for consultant work. The conceptualization, study design, data collection, analysis, and interpretation, decision to publish, and manuscript preparation were performed by the authors independently of Novocure. D.C. and D.D.T. are inventors of 2 patent applications related to work reported in this paper; however, royalty-free commercialization rights were transferred to Novocure per the funding agreement. D.D.T. has also received research funding from Merck, Sarepta, Novartis, Monteris, and Lacerta for other unrelated work. A.P.G. has received personal honoraria for consultant work from Alexion Pharmaceuticals, Servier, ONO Pharma USA, Monteris Medical, Neosoma, Aptitude Health, Guidepoint. A.P.G. has held personal stock in Viatris.

STAR★METHODS

Detailed methods are provided in the online version of this paper and include the following:

- KEY RESOURCES TABLE
- EXPERIMENTAL MODEL AND STUDY PARTICIPANT DETAILS
  - Approval
  - Participant population detail
- METHOD DETAILS
  - Treatment plan
  - Assessment
- QUANTIFICATION AND STATISTICAL ANALYSIS
  - Case-matched control cohort
  - Bulk RNA-seq of enriched T lymphocytes
  - Single cell RNA-seq (scRNA-seq) analysis of PBMCs
  - TCR clonotyping
  - External dataset
  - Immunohistochemistry

SUPPLEMENTAL INFORMATION

Supplemental information can be found online at https://doi.org/10.1016/j.medj.2025.100708.

Received: April 11, 2025
Revised: April 29, 2025
Accepted: May 2, 2025
Published: June 3, 2025

REFERENCES

1. Stupp, R., Taillibert, S., Kanner, A., Read, W., Steinberg, D., Lhermitte, B., Toms, S., Idbaih, A., Ahluwalia, M.S., Fink, K., et al. (2017). Effect of tumor-treating fields plus maintenance temozolomide vs maintenance temozolomide alone on survival in patients with glioblastoma: a randomized clinical trial. JAMA *318*, 2306–2316. https://doi.org/10.1001/jama.2017.18718.
2. Cahill, D.P. (2021). Extent of Resection of Glioblastoma: A Critical Evaluation in the Molecular Era. Neurosurg. Clin. N. Am. *32*, 23–29. https://doi.org/10.1016/j.nec.2020.09.006.
3. Löber-Handwerker, R., Döring, K., Bock, C., Rohde, V., and Malinova, V. (2022). Defining the impact of adjuvant treatment on the prognosis of patients with inoperable glioblastoma undergoing biopsy only: does the survival benefit outweigh the treatment effort? Neurosurg. Rev. *45*, 2339–2347. https://doi.org/10.1007/s10143-022-01754-y.
4. Harlay, V., Appay, R., Bequet, C., Petrirena, G., Campello, C., Barrié, M., Autran, D., Graillon, T., Boissonneau, S., Dufour, H., et al. (2023). Radiochemotherapy feasibility for biopsy-only unresectable IDH wild-type glioblastomas (BO-GBM). Neuro-Oncol. Pract. *10*, 536–543. https://doi.org/10.1093/nop/npad028.
5. Robert, C. (2020). A decade of immune-checkpoint inhibitors in cancer therapy. Nat. Commun. *11*, 3801. https://doi.org/10.1038/s41467-020-17670-y.
6. Medikonda, R., Dunn, G., Rahman, M., Fecci, P., and Lim, M. (2021). A review of glioblastoma immunotherapy. J. Neuro Oncol. *151*, 41–53. https://doi.org/10.1007/s11060-020-03448-1.
7. Arrieta, V.A., Dmello, C., McGrail, D.J., Brat, D.J., Lee-Chang, C., Heimberger, A.B., Chand, D., Stupp, R., and Sonabend, A.M. (2023). Immune checkpoint blockade in glioblastoma: from tumor heterogeneity to personalized treatment. J. Clin. Investig. *133*, e163447. https://doi.org/10.1172/JCI163447.
8. Lim, M., Weller, M., Idbaih, A., Steinbach, J., Finocchiaro, G., Raval, R.R., Ansstas, G., Baehring, J., Taylor, J.W., Honnorat, J., et al. (2022). Phase III trial of chemoradiotherapy with temozolomide plus nivolumab or placebo for newly diagnosed glioblastoma with methylated MGMT promoter. Neuro Oncol. *24*, 1935–1949. https://doi.org/10.1093/neuonc/noac116.
9. Omuro, A., Brandes, A.A., Carpentier, A.F., Idbaih, A., Reardon, D.A., Cloughesy, T., Sumrall, A., Baehring, J., van den Bent, M., Bähr, O., et al. (2023). Radiotherapy combined with nivolumab or temozolomide for newly diagnosed glioblastoma with unmethylated MGMT promoter: An international randomized phase III trial. Neuro Oncol. *25*, 123–134. https://doi.org/10.1093/neuonc/noac099.
10. Sampson, J.H., Gunn, M.D., Fecci, P.E., and Ashley, D.M. (2020). Brain immunology and immunotherapy in brain tumours. Nat. Rev. Cancer *20*, 12–25. https://doi.org/10.1038/s41568-019-0224-7.
11. Jackson, C.M., Choi, J., and Lim, M. (2019). Mechanisms of immunotherapy resistance: lessons from glioblastoma. Nat. Immunol. *20*, 1100–1109. https://doi.org/10.1038/s41590-019-0433-y.
12. Havel, J.J., Chowell, D., and Chan, T.A. (2019). The evolving landscape of biomarkers for checkpoint inhibitor immunotherapy. Nat. Rev. Cancer *19*, 133–150. https://doi.org/10.1038/s41568-019-0116-x.
13. van Solinge, T.S., Nieland, L., Chiocca, E.A., and Broekman, M.L.D. (2022). Advances in local therapy for glioblastoma — taking the fight to the tumour. Nat. Rev. Neurol. *18*, 221–236. https://doi.org/10.1038/s41582-022-00621-0.
14. Nassiri, F., Patil, V., Yefet, L.S., Singh, O., Liu, J., Dang, R.M.A., Yamaguchi, T.N., Daras, M., Cloughesy, T.F., Colman, H., et al. (2023). Oncolytic DNX-2401 virotherapy plus pembrolizumab in recurrent glioblastoma: a

phase 1/2 trial. Nat. Med. *29*, 1370–1378. https://doi.org/10.1038/s41591-023-02347-y.

15. Shin, D.H., Melnick, K.F., Tran, D.D., and Ghiaseddin, A.P. (2021). In situ vaccination with laser interstitial thermal therapy augments immunotherapy in malignant gliomas. J. Neuro Oncol. *151*, 85–92. https://doi.org/10.1007/s11060-020-03557-x.
16. Moser, J.C., Salvador, E., Deniz, K., Swanson, K., Tuszynski, J., Carlson, K.W., Karanam, N.K., Patel, C.B., Story, M., Lou, E., and Hagemann, C. (2022). The Mechanisms of Action of Tumor Treating Fields. Cancer Res. *82*, 3650–3658. https://doi.org/10.1158/0008-5472.Can-22-0887.
17. Voloshin, T., Kaynan, N., Davidi, S., Porat, Y., Shteingauz, A., Schneiderman, R.S., Zeevi, E., Munster, M., Blat, R., Tempel Brami, C., et al. (2020). Tumor-treating fields (TTFields) induce immunogenic cell death resulting in enhanced antitumor efficacy when combined with anti-PD-1 therapy. Cancer Immunol. Immunother. *69*, 1191–1204. https://doi.org/10.1007/s00262-020-02534-7.
18. Barsheshet, Y., Voloshin, T., Brant, B., Cohen, G., Koren, L., Blatt, R., Cahal, S., Haj Khalil, T., Zemer Tov, E., Paz, R., et al. (2022). Tumor Treating Fields (TTFields) Concomitant with Immune Checkpoint Inhibitors Are Therapeutically Effective in Non-Small Cell Lung Cancer (NSCLC) In Vivo Model. Int. J. Mol. Sci. *23*, 14073. https://doi.org/10.3390/ijms232214073.
19. Chen, D., Le, S.B., Hutchinson, T.E., Calinescu, A.A., Sebastian, M., Jin, D., Liu, T., Ghiaseddin, A., Rahman, M., and Tran, D.D. (2022). Tumor Treating Fields dually activate STING and AIM2 inflammasomes to induce adjuvant immunity in glioblastoma. J. Clin. Investig. *132*, e149258. https://doi.org/10.1172/JCI149258.
20. Leal, T., Kotecha, R., Ramlau, R., Zhang, L., Milanowski, J., Cobo, M., Roubec, J., Petruzelka, L., Havel, L., Kalmadi, S., et al. (2023). Tumor Treating Fields therapy with standard systemic therapy versus standard systemic therapy alone in metastatic non-small-cell lung cancer following progression on or after platinum-based therapy (LUNAR): a randomised, open-label, pivotal phase 3 study. Lancet Oncol. *24*, 1002–1017. https://doi.org/10.1016/s1470-2045(23)00344-3.
21. Okada, H., Weller, M., Huang, R., Finocchiaro, G., Gilbert, M.R., Wick, W., Ellingson, B.M., Hashimoto, N., Pollack, I.F., Brandes, A.A., et al. (2015). Immunotherapy response assessment in neuro-oncology: a report of the RANO working group. Lancet Oncol. *16*, e534–e542. https://doi.org/10.1016/S1470-2045(15)00088-1.
22. Louis, D.N., Perry, A., Wesseling, P., Brat, D.J., Cree, I.A., Figarella-Branger, D., Hawkins, C., Ng, H.K., Pfister, S.M., Reifenberger, G., et al. (2021). The 2021 WHO Classification of Tumors of the Central Nervous System: a summary. Neuro Oncol. *23*, 1231–1251. https://doi.org/10.1093/neuonc/noab106.
23. Eckel-Passow, J.E., Lachance, D.H., Molinaro, A.M., Walsh, K.M., Decker, P.A., Sicotte, H., Pekmezci, M., Rice, T., Kosel, M.L., Smirnov, I.V., et al. (2015). Glioma Groups Based on 1p/19q. N. Engl. J. Med. *372*, 2499–2508. https://doi.org/10.1056/NEJMoa1407279.
24. Louis, D.N., Perry, A., Reifenberger, G., von Deimling, A., Figarella-Branger, D., Cavenee, W.K., Ohgaki, H., Wiestler, O.D., Kleihues, P., and Ellison, D.W. (2016). The 2016 World Health Organization Classification of Tumors of the Central Nervous System: a summary. Acta Neuropathol. *131*, 803–820. https://doi.org/10.1007/s00401-016-1545-1.
25. Butler, A., Hoffman, P., Smibert, P., Papalexi, E., and Satija, R. (2018). Integrating single-cell transcriptomic data across different conditions, technologies, and species. Nat. Biotechnol. *36*, 411–420. https://doi.org/10.1038/nbt.4096.
26. Stuart, T., Butler, A., Hoffman, P., Hafemeister, C., Papalexi, E., Mauck, W. M., III, Hao, Y., Stoeckius, M., Smibert, P., and Satija, R. (2019). Comprehensive Integration of Single-Cell Data. Cell *177*, 1888–1902.e21. https://doi.org/10.1016/j.cell.2019.05.031.
27. Becht, E., McInnes, L., Healy, J., Dutertre, C.-A., Kwok, I.W.H., Ng, L.G., Ginhoux, F., and Newell, E.W. (2018). Dimensionality reduction for visualizing single-cell data using UMAP. Nat. Biotechnol. *37*, 38–44. https://doi.org/10.1038/nbt.4314.
28. Greiff, V., Bhat, P., Cook, S.C., Menzel, U., Kang, W., and Reddy, S.T. (2015). A bioinformatic framework for immune repertoire diversity profiling enables detection of immunological status. Genome Med. *7*, 49. https://doi.org/10.1186/s13073-015-0169-8.
29. Yost, K.E., Satpathy, A.T., Wells, D.K., Qi, Y., Wang, C., Kageyama, R., McNamara, K.L., Granja, J.M., Sarin, K.Y., Brown, R.A., et al. (2019). Clonal replacement of tumor-specific T cells following PD-1 blockade. Nat. Med. *25*, 1251–1259. https://doi.org/10.1038/s41591-019-0522-3.
30. Liu, B., Hu, X., Feng, K., Gao, R., Xue, Z., Zhang, S., Zhang, Y., Corse, E., Hu, Y., Han, W., and Zhang, Z. (2022). Temporal single-cell tracing reveals clonal revival and expansion of precursor exhausted T cells during anti-PD-1 therapy in lung cancer. Nat. Cancer *3*, 108–121. https://doi.org/10.1038/s43018-021-00292-8.
31. Aggarwal, C., Ben-Shachar, R., Gao, Y., Hyun, S.W., Rivers, Z., Epstein, C., Kaneva, K., Sangli, C., Nimeiri, H., and Patel, J. (2023). Assessment of Tumor Mutational Burden and Outcomes in Patients With Diverse Advanced Cancers Treated With Immunotherapy. JAMA Netw. Open *6*, e2311181. https://doi.org/10.1001/jamanetworkopen.2023.11181.
32. Śledzińska, P., Bebyn, M.G., Furtak, J., Kowalewski, J., and Lewandowska, M.A. (2021). Prognostic and Predictive Biomarkers in Gliomas. Int. J. Mol. Sci. *22*, 10373. https://doi.org/10.3390/ijms221910373.
33. Huang, R., and Zhou, P.-K. (2021). DNA damage repair: historical perspectives, mechanistic pathways and clinical translation for targeted cancer therapy. Signal Transduct. Target. Ther. *6*, 254. https://doi.org/10.1038/s41392-021-00648-7.
34. Li, Z., Bao, S., Wu, Q., Wang, H., Eyler, C., Sathornsumetee, S., Shi, Q., Cao, Y., Lathia, J., McLendon, R.E., et al. (2009). Hypoxia-inducible factors regulate tumorigenic capacity of glioma stem cells. Cancer Cell *15*, 501–513. https://doi.org/10.1016/j.ccr.2009.03.018.
35. Krishna, S., Choudhury, A., Keough, M.B., Seo, K., Ni, L., Kakaizada, S., Lee, A., Aabedi, A., Popova, G., Lipkin, B., et al. (2023). Glioblastoma remodelling of human neural circuits decreases survival. Nature *617*, 599–607.
36. Woroniecka, K., Chongsathidkiet, P., Rhodin, K., Kemeny, H., Dechant, C., Farber, S.H., Elsamadicy, A.A., Cui, X., Koyama, S., Jackson, C., et al. (2018). T-Cell Exhaustion Signatures Vary with Tumor Type and Are Severe in Glioblastoma. Clin. Cancer Res. *24*, 4175–4186. https://doi.org/10.1158/1078-0432.Ccr-17-1846.
37. Tomaszewski, W., Sanchez-Perez, L., Gajewski, T.F., and Sampson, J.H. (2019). Brain Tumor Microenvironment and Host State: Implications for Immunotherapy. Clin. Cancer Res. *25*, 4202–4210. https://doi.org/10.1158/1078-0432.CCR-18-1627.
38. Liu, T., Jin, D., Le, S.B., Chen, D., Sebastian, M., Riva, A., Liu, R., and Tran, D.D. (2024). Machine Learning-Directed Conversion of Glioblastoma Cells to Dendritic Cell-like Antigen-Presenting Cells as Cancer Immunotherapy. Cancer Immunol. Res. *12*, 1340–1360. https://doi.org/10.1158/2326-6066.Cir-23-0721.
39. Himes, B.T., Geiger, P.A., Ayasoufi, K., Bhargav, A.G., Brown, D.A., and Parney, I.F. (2021). Immunosuppression in Glioblastoma: Current Understanding and Therapeutic Implications. Front. Oncol. *11*, 770561. https://doi.org/10.3389/fonc.2021.770561.
40. Sattiraju, A., Kang, S., Giotti, B., Chen, Z., Marallano, V.J., Brusco, C., Ramakrishnan, A., Shen, L., Tsankov, A.M., Hambardzumyan, D., et al. (2023). Hypoxic niches attract and sequester tumor-associated macrophages and cytotoxic T cells and reprogram them for immunosuppression. Immunity *56*, 1825–1843.e6. https://doi.org/10.1016/j.immuni.2023.06.017.
41. Colella, B., Faienza, F., and Di Bartolomeo, S. (2019). EMT Regulation by Autophagy: A New Perspective in Glioblastoma Biology. Cancers (Basel) *11*, 312. https://doi.org/10.3390/cancers11030312.
42. Venkataramani, V., Yang, Y., Schubert, M.C., Reyhan, E., Tetzlaff, S.K., Wißmann, N., Botz, M., Soyka, S.J., Beretta, C.A., Pramatarov, R.L., et al. (2022). Glioblastoma hijacks neuronal mechanisms for brain invasion. Cell *185*, 2899–2917.e31. https://doi.org/10.1016/j.cell.2022.06.054.

43. Winkler, F., Venkatesh, H.S., Amit, M., Batchelor, T., Demir, I.E., Deneen, B., Gutmann, D.H., Hervey-Jumper, S., Kuner, T., Mabbott, D., et al. (2023). Cancer neuroscience: State of the field, emerging directions. Cell *186*, 1689–1707. https://doi.org/10.1016/j.cell.2023.02.002.

44. Chen, D., Le, S.B., Manektalia, H., Liu, T., Hutchinson, T.E., O'Dell, A., Salhia, B., and Tran, D.D. (2024). The EP3–ZNF488 Axis Promotes Self-Renewal of Glioma Stem-like Cells to Induce Resistance to Tumor Treating Fields. Cancer Res. *85*, 360–377. https://doi.org/10.1158/0008-5472.Can-23-3643.

45. Sheng, Z., Li, L., Zhu, L.J., Smith, T.W., Demers, A., Ross, A.H., Moser, R.P., and Green, M.R. (2010). A genome-wide RNA interference screen reveals an essential CREB3L2-ATF5-MCL1 survival pathway in malignant glioma with therapeutic implications. Nat. Med. *16*, 671–677.

46. Wang, L.-B., Karpova, A., Gritsenko, M.A., Kyle, J.E., Cao, S., Li, Y., Rykunov, D., Colaprico, A., Rothstein, J.H., Hong, R., et al. (2021). Proteogenomic and metabolomic characterization of human glioblastoma. Cancer Cell *39*, 509–528.e20. https://doi.org/10.1016/j.ccell.2021.01.006.

47. Quan, Z., Yang, Y., Zheng, H., Zhan, Y., Luo, J., Ning, Y., and Fan, S. (2022). Clinical implications of the interaction between PD-1/PD-L1 and PI3K/AKT/mTOR pathway in progression and treatment of non-small cell lung cancer. J. Cancer *13*, 3434–3443. https://doi.org/10.7150/jca.77619.

48. Bai, X., Wang, X., Ma, G., Song, J., Liu, X., Wu, X., Zhao, Y., Liu, X., Liu, Z., Zhang, W., et al. (2021). Improvement of PD-1 Blockade Efficacy and Elimination of Immune-Related Gastrointestinal Adverse Effect by mTOR Inhibitor. Front. Immunol. *12*, 793831. https://doi.org/10.3389/fimmu.2021.793831.

49. Ward-Kavanagh, L.K., Lin, W.W., Šedý, J.R., and Ware, C.F. (2016). The TNF Receptor Superfamily in Co-stimulating and Co-inhibitory Responses. Immunity *44*, 1005–1019. https://doi.org/10.1016/j.immuni.2016.04.019.

50. Bertrand, F., Rochotte, J., Colacios, C., Montfort, A., Tilkin-Mariamé, A.-F., Touriol, C., Rochaix, P., Lajoie-Mazenc, I., Andrieu-Abadie, N., Levade, T., et al. (2015). Blocking Tumor Necrosis Factor α Enhances CD8 T-cell–Dependent Immunity in Experimental Melanoma. Cancer Res. *75*, 2619–2628. https://doi.org/10.1158/0008-5472.Can-14-2524.

51. Koyama, S., Akbay, E.A., Li, Y.Y., Herter-Sprie, G.S., Buczkowski, K.A., Richards, W.G., Gandhi, L., Redig, A.J., Rodig, S.J., Asahina, H., et al. (2016). Adaptive resistance to therapeutic PD-1 blockade is associated with upregulation of alternative immune checkpoints. Nat. Commun. *7*, 10501. https://doi.org/10.1038/ncomms10501.

52. Wei, S.C., Duffy, C.R., and Allison, J.P. (2018). Fundamental Mechanisms of Immune Checkpoint Blockade Therapy. Cancer Discov. *8*, 1069–1086. https://doi.org/10.1158/2159-8290.Cd-18-0367.

53. Diamant, G., Simchony Goldman, H., Gasri Plotnitsky, L., Roitman, M., Shiloach, T., Globerson-Levin, A., Eshhar, Z., Haim, O., Pencovich, N., Grossman, R., et al. (2021). T Cells Retain Pivotal Antitumoral Functions under Tumor-Treating Electric Fields. J. Immunol. *207*, 709–719. https://doi.org/10.4049/jimmunol.2100100.

54. Ostrom, Q.T., Cioffi, G., Gittleman, H., Patil, N., Waite, K., Kruchko, C., and Barnholtz-Sloan, J.S. (2019). CBTRUS Statistical Report: Primary Brain and Other Central Nervous System Tumors Diagnosed in the United States in 2012-2016. Neuro Oncol. *21*, v1–v100. https://doi.org/10.1093/neuonc/noz150.

55. Stupp, R., Wong, E.T., Kanner, A.A., Steinberg, D., Engelhard, H., Heidecke, V., Kirson, E.D., Taillibert, S., Liebermann, F., Dbalý, V., et al. (2012). NovoTTF-100A versus physician's choice chemotherapy in recurrent glioblastoma: a randomised phase III trial of a novel treatment modality. Eur. J. Cancer *48*, 2192–2202. https://doi.org/10.1016/j.ejca.2012.04.011.

56. Simnica, D., Akyüz, N., Schliffke, S., Mohme, M., v.Wenserski, L., Mährle, T., Fanchi, L.F., Lamszus, K., and Binder, M. (2019). T cell receptor next-generation sequencing reveals cancer-associated repertoire metrics and reconstitution after chemotherapy in patients with hematological and solid tumors. OncoImmunology *8*, e1644110. https://doi.org/10.1080/2162402X.2019.1644110.

57. Sampson, J.H., Aldape, K.D., Archer, G.E., Coan, A., Desjardins, A., Friedman, A.H., Friedman, H.S., Gilbert, M.R., Herndon, J.E., McLendon, R.E., et al. (2011). Greater chemotherapy-induced lymphopenia enhances tumor-specific immune responses that eliminate EGFRvIII-expressing tumor cells in patients with glioblastoma. Neuro Oncol. *13*, 324–333. https://doi.org/10.1093/neuonc/noq157.

58. Karachi, A., Dastmalchi, F., Mitchell, D.A., and Rahman, M. (2018). Temozolomide for immunomodulation in the treatment of glioblastoma. Neuro Oncol. *20*, 1566–1572. https://doi.org/10.1093/neuonc/noy072.

59. Grossman, S.A., Ye, X., Lesser, G., Sloan, A., Carraway, H., Desideri, S., and Piantadosi, S.; NABTT CNS Consortium (2011). Immunosuppression in Patients with High-Grade Gliomas Treated with Radiation and Temozolomide. Clin. Cancer Res. *17*, 5473–5480. https://doi.org/10.1158/1078-0432.Ccr-11-0774.

60. Karachi, A., Yang, C., Dastmalchi, F., Sayour, E.J., Huang, J., Azari, H., Long, Y., Flores, C., Mitchell, D.A., and Rahman, M. (2019). Modulation of temozolomide dose differentially affects T-cell response to immune checkpoint inhibition. Neuro Oncol. *21*, 730–741. https://doi.org/10.1093/neuonc/noz015.

61. Chaudhry, A., Benson, L., Varshaver, M., Farber, O., Weinberg, U., Kirson, E., and Palti, Y. (2015). NovoTTF-100A System (Tumor Treating Fields) transducer array layout planning for glioblastoma: a NovoTAL system user study. World J. Surg. Oncol. *13*, 316. https://doi.org/10.1186/s12957-015-0722-3.

62. Wu, J., and Xiong, X. (2015). Group Sequential Design for Randomized Phase III Trials under the Weibull Model. J. Biopharm. Stat. *25*, 1190–1205. https://doi.org/10.1080/10543406.2014.971165.

63. Hegde, S., Krisnawan, V.E., Herzog, B.H., Zuo, C., Breden, M.A., Knolhoff, B.L., Hogg, G.D., Tang, J.P., Baer, J.M., Mpoy, C., et al. (2020). Dendritic Cell Paucity Leads to Dysfunctional Immune Surveillance in Pancreatic Cancer. Cancer Cell *37*, 289–307.e9. https://doi.org/10.1016/j.ccell.2020.02.008.

64. Abeysekera, W., and Sooriyarachchi, M. (2009). Use of Schoenfeld's global test to test the proportional hazards assumption in the Cox proportional hazards model: an application to a clinical study. J. Natl. Sci. Found. *37*, 41.

STAR★METHODS

KEY RESOURCES TABLE

REAGENT or RESOURCE	SOURCE	IDENTIFIER
Antibodies		
Anti-LGALS9 antibody	Sigma-Aldrich	Cat#MABT833; RRID: AB_3696950
Anti-PD-L1 antibody	Abcam	Cat#AB205921; RRID: AB_2687878
Anti-VSIR antibody	Abcam	Cat#AB300042; RRID: AB_3696949
Biological samples		
Patient tumor tissues (GBM)	University of Florida/USC Brain Tumor Center	N/A
Patient PBMC samples	University of Florida/USC Brain Tumor Center	N/A
Critical commercial assays		
Human Pan T cell Isolation Kit	Miltenyi Biotec	Cat#130-096-535
QIAGEN RNeasy Midi Kit	QIAGEN	Cat#75144
QIAGEN RNeasy FFPE Kit	QIAGEN	Cat#73504
Chromium Next GEM Single Cell 5′ v2 (Dual Index)	10x Genomics	Cat#PN-1000263
Human V(D)J Amplification Kit	10x Genomics	Cat#PN-1000252
Deposited data		
Raw and analyzed data	This paper	GEO: GSE269869, GSE269956, GSE269957
Bulk RNA-seq dataset for chemoradiation/TTFields	European Genome-phenome Archive	EGAC00001002176
Software and algorithms		
Seurat R package (v3.2.2)	Butler et al., Stuart et al.[25,26]	https://satijalab.org/seurat/
Cell Ranger (v7.0.0)	10x Genomics	https://support.10xgenomics.com/
ImmunoArch R package (v0.9.0)	Immunoarch Team	https://cloud.r-project.org/web/packages/immunarch/index.html
GeneRep-nSCORE platform	Liu et al.[38]	https://github.com/TranLabUSC/NETZEN-classic
Custom Analysis Pipelines	This paper	https://github.com/TranLabUSC/2TT_clinical_trial_paper
Cytoscape software (v3.10.0)	Cytoscape Consortium	https://cytoscape.org
Blender (v3.6)	Blender Foundation	https://www.blender.org

EXPERIMENTAL MODEL AND STUDY PARTICIPANT DETAILS

Approval

Human subject work was performed in accordance with an approved protocol from the IRB at the University of Florida and the University of Southern California—ClinicalTrials.gov ID NCT03405792. An informed consent was obtained from each human participant before study procedures and analysis were performed. All enrollments were completed at the University of Florida.

Participant population detail

Participants information on sex, age, and race was self-reported. Information on gender and socioeconomic status was not collected. Adult patients, who had histologically confirmed GBM, WHO grade IV—GBM variants were allowed—KPS of at least 70%, had maximal safe resection of primary tumor including biopsy only, had completed standard radiotherapy with concurrent TMZ, required no more than 4mg daily dexamethasone, and had adequate bone marrow and organ functions, were eligible. Histopathologic confirmation was performed at the University of Florida Neuropathology Division. MGMT promoter methylation status was determined centrally at LabCorp using the quantitative methylation-specific PCR (qMSP) method. Starting in 2021—in 2020 at our own institution—important updates to the WHO CNS tumors classification were instituted that eliminated IDH1/2 mutant tumors from the GBM classification.[22] As a result, the last 8 enrollments included only wt-IDH GBM. While Gliadel wafers were allowed at the time of surgical resection of the primary tumors, none of the enrolled subjects received this treatment. Those, who had received anti-angiogenic agents, anti-PD-1 and other ICIs, had progressive disease per iRANO criteria, multifocal gliomas defined as distinct

tumors without overlapping T2/FLAIR signal, leptomeningeal metastases, a history of immunodeficiency or autoimmune disease requiring systemic treatment within the previous 2 years, known history of HIV, active hepatitis B, active hepatitis C, and active tuberculosis, and were pregnant or unwilling to use an acceptable method of contraception, were excluded. The complete inclusion and exclusion criteria are listed in the STAR Methods.

METHOD DETAILS

Treatment plan

Patients were treated with a minimum of 6 and maximum of 12 cycles of adjuvant TMZ depending on tolerability and toxicity—cycle 1 dosed at 150 mg/m^2 daily for 5 days on a 28-day cycle was started at least 4 but no later than 6 weeks from the end of chemoradiation, which was increased to 200 mg/m^2 daily for 5 days starting with cycle 2 of TMZ. Continuous TTFields began with cycle 1 of TMZ and pembrolizumab 200 mg intravenously every 3 weeks was added starting with cycle 2 of TMZ. The minimum usage of the TTFields device (Optune) was 50% of time averaged over each 4-week period with the goal of 75% usage time. TTFields delivery using transducer arrays was achieved using array layouts and placement according to the approved clinical NovoTAL mapping system based on individual patient's head geometry and the lesion's location, size, and shape on brain MRI.[61] Both TTFields and pembrolizumab treatments were administered for up to 2 years or until disease progression or excessive toxicity, whichever occurred first. Patients were allowed to continue TTFields treatment past the first recurrence until the second recurrence. Long-term survivors could continue TTFields or pembrolizumab or both past 2 years on an individual basis.

Assessment

Patients were monitored closely for the duration of the study to ensure safety. AEs and SAEs were documented and graded according to the Common Terminology Criteria for Adverse Events (CTCAE), v.4 with clear assignment of relatedness to the study treatment. Dexamethasone dose was monitored at each monthly visit. Disease assessment was performed using the iRANO criteria.[21] A baseline brain MRI was performed at enrollment and repeated every 2 months until disease progression or at the end of study treatment at 2 years, whichever occurred first. To determine the immune signature of response, we collected blood samples for bulk and single cell RNA-seq analysis of PBMC at the following time points: before TTFields (Pre-TTF), 4 weeks after TTFields (Post-TTF and before cycle 1 of pembrolizumab), before cycles 2, 4, 9, 17, and 34 of pembrolizumab, and at the time of tumor recurrence. Primary tumor samples and recurrent tumors (if available) were obtained for bulk RNA-seq, whole exome sequencing and IHC analyses.

QUANTIFICATION AND STATISTICAL ANALYSIS

The primary objective was PFS. The secondary objectives were OS, safety, objective response, and immune response signatures. Survival endpoints were defined as the time from study enrollment to the survival events at the data cutoff date. Patients who are lost to follow-up and the patients who are still alive at the date of data cutoff will be censored at the date the patient was last known alive or the cutoff date, whichever occurs first. Power calculation based on a one-sided, one-sample log-rank test shows that with sample size of 24 patients, this study achieves over 80% power at a 0.05 significance level to detect an improvement in median PFS by 6 months for the treatment group (i.e., the triple regimen of TTFields, pembrolizumab and TMZ), when the median survival time of the historic control group is 6.7 months (i.e., TTFields plus TMZ arm in the EF-14 study). It is assumed that the survival time distributions of both groups are approximated reasonably well by the Weibull distribution with a shape parameter of 0.88.[62] Patients were stratified for MGMT promoter methylation and extent of tumor resection for survival analysis. We applied the log rank test to evaluate survival patterns between the maximal tumor resection and biopsy-only groups through Kaplan-Meier curves and incorporated the 95% confidence intervals (CI). The estimated median survival probability is reported along with the corresponding 95% CI. Best responses were measured per iRANO criteria.[21] A complete response (CR) was defined as the disappearance of all enhancing measurable and non-measurable disease on a stable or decreasing steroid dose and sustained for at least 30 days. A partial response (PR) was defined as a $\geq$50% decrease in the sum of the products of perpendicular diameters of all measurable enhancing lesions on a stable or decreasing steroid dose and sustained for at least 30 days. Patients with disease progression could continue with study treatment if deemed safe and would have a repeat brain MRI within 4 weeks to confirm progression. Various computational methods were used to analyze the genomics data obtained as detailed below.

Case-matched control cohort

To identify a suitable control group for the 2-THE-TOP study, 152 patients from the experimental arm (TTFields + TMZ) of the EF-14 trial[1] were initially pre-selected based on the following criteria, matching those of the 2-THE-TOP study (Table S1).

(1) TTFields usage $\geq$ 50%.
(2) TTFields duration $\geq$ 4 weeks.
(3) Available IDH and MGMT assessment.
(4) Baseline KPS score $\geq$ 70.
(5) Similar follow up time.

However, the 26 patients enrolled in the 2-THE-TOP study exhibited notable baseline imbalances compared to the overall EF-14 population. Specifically, 27% of 2-THE-TOP patients underwent only a biopsy at initial diagnosis (all with a KPS score of 80), whereas in EF-14, approximately 15% were biopsy-only patients (and only 5% had a KPS score of 80). Imbalances were also evident in KPS score, MGMT status, and other variables across resection status. Given the small sample size and pronounced data imbalance, propensity score matching was not feasible because it can increase bias under such conditions.

To address these imbalances, the EF-14 data were divided into smaller subgroups. The initial stratification was based on KPS score and extent of resection, but to achieve a closer match to the 2-THE-TOP population, additional variables (e.g., MGMT, IDH mutation status, and age) were also considered. When a particular subgroup in EF-14 was smaller than the corresponding subgroup in 2-THE-TOP, the entire EF-14 subgroup was included (e.g., the "biopsy with KPS = 80" category, which comprised only 7 out of the 152 pre-selected EF-14 patients [4.6%]). If an EF-14 subgroup was larger, random selection using the SURVEYSELECT procedure in SAS was applied to attain the appropriate proportion.

Following this subgroup selection and proportional matching process, a simulation was performed to determine the maximum number of EF-14 controls that could be included without significantly altering the distribution of key variables. An exact chi-square test ensured the *p*-value remained above 0.1, maintaining the distribution balance.

Ultimately, this approach yielded a final control cohort of 56 patients from the EF-14 study for statistical analyses.

Bulk RNA-seq of enriched T lymphocytes

Sample processing

Using the human pan T cell isolation kit (Miltenyi Biotec, Cat#130-096-535), untouched T cells were isolated from the PBMC single-cell suspensions in accordance with the manufacturer's guidelines. RNA extraction was performed using the QIAGEN RNeasy Midi Kit (Cat#75144), following the protocols provided by the manufacturer. Total tumor RNA was extracted from snap frozen and formalin—fixed paraffin—embedded tumor samples using QIAGEN RNeasy Midi Kit (Cat#75144) and RNeasy FFPE Kit (Cat#73504) separately. The bulk RNA-seq library construction, pooling, and sequencing were executed by NOVOGENE.

Pathway differential expression analysis

Gene Set Enrichment Analysis (GSEA) was employed for the investigation of specific immune pathways of interest. In the context of comparing Maximal Resection versus Biopsy Only conditions, genes were ranked based on their log Foldchange derived from Gene differential expression analysis outcomes. Subsequently, GSEA in the pre-ranked "classic" mode with 10,000 permutations was executed to ascertain the enrichment of desired pathways. The necessary command lines and the Java implementation for GSEA were acquired from the Broad Institute's software portal http://software.broadinstitute.org/gsea/index.jsp.

Boxplots for pathway activity

For each pathway among the top 10 identified via GSEA, boxplots were created to elucidate differences in pathway activity between samples from Maximal Resection and Biopsy Only groups across various timepoints. The calculation of pathway activity was based on the average expression values of genes constituting a pathway, with the relevant pathway gene sets being procured from the GSEA-MSigDB website http://www.gsea-msigdb.org.

Differential expression network analysis

The differential expression network analysis was performed using the GeneRep/nSCORE platform as previously described.[38] The 3D GeneRep/nSCORE analysis plot was created by Blender (v 3.6). The gene interactions networks were generated using publicly available dataset.[38] The 2D gene network was visualized using Cytoscape software (v. 3.10.0).

Single cell RNA-seq (scRNA-seq) analysis of PBMCs

Sample processing

Cryopreserved PBMCs obtained from patients were rinsed in PBS, and cell viability was assessed using Trypan Blue staining. Single-cell suspensions were then prepared and applied to the Chromium Single Cell Chip (10x Genomics) as per the instructions provided by the manufacturer. Subsequently, single-cell RNA-seq libraries were generated using the Chromium Next GEM Single Cell 5′ v2 (Dual Index). To ensure consistency, all patient samples and the corresponding libraries were processed simultaneously in a single batch. Sequencing of the single-cell libraries was performed on an Illumina NovaSeq system, utilizing an 8-base i7 sample index read, a 28-base read 1 for capturing cell barcodes and unique molecular identifiers (UMIs), and a 150-base read 2 for the mRNA insert.

Data processing

The main operations were performed using the Seurat R package (3.2.2),[25,26] unless otherwise stated. When option parameters for function deviated from the default values, we provided details of the changes accordingly. Most of the changes to the default options were made to accommodate and leverage the large size of the dataset. Cell Ranger Aggregation: The raw sequencing data was processed using cellranger mkfastq and cellranger multi commands of Cell Ranger package as described in TCR clonotyping section. Results from all libraries and batches were pooled together using the command cellranger aggr without normalization for dead cells as it will be handled downstream. The filtered background feature barcode matrix obtained from this step was used as input for sequential analysis. Normalization of UMI: Using the global scaling normalization method, the feature expression for each cell was divided by the total expression, multiplied by the scale factor (10,000), and log transformed using the Seurat R function NormalizeData with method "Log Normalize". Seurat aggregation and correction for batch effect: As the counts were from three different batches, to align cells and eliminate batch effects for dimension reduction and clustering, we adopted the multi dataset

integration strategy as previously described.[26] Briefly, "anchors cells" were identified between pairs of datasets and used to normalize multiple datasets from different batches. We chose a reference based, reciprocal PCA variant of the method detailed in the Seurat R package.[25,26] First, we split the previously integrated dataset by batches, using the Seurat function SplitObject. Next, for each split object, we performed variable feature selection using the function FindVariableFeatures. Features for integration were selected using the function SelectIntegrationFeatures and PCA performed for each split object on the selected features. The anchor cells were identified by using the function FindIntegrationAnchors with the reference chosen as the largest among 3 batches and the reduction option set to 'rpca'. Finally, the whole datasets from 3 batches were reintegrated using the function IntegrateData with the identified anchor cells.

Uniform Manifold Approximation and Projection (UMAP) dimension reduction: The integrated multiple batch dataset was used as input for UMAP dimension reduction.[27] The feature expression was scaled using the Seurat function ScaleData, followed by a PCA run using the function RunPCA (Seurat) with the total number of principal components (PC) to compute and store option of 100. The UMAP coordinates for single cells were obtained using the RunUMAP function (Seurat) with the top 75 PCs as input features (dims = 1:75) with min.dist = 0.75 and the number of training epochs n.epochs = 2000. Clustering of cells: We relied on a graph-based clustering approach implemented in the Seurat package, which embeds cells in a K-nearest neighbor graph with edges drawn between similar cells and partitions nodes in the network into communities. Briefly, a Shared Nearest Neighbor graph was constructed using the FindNeigbhors function with an option dimension of reduction input dims = 1:75, error bound nn.eps = 0.5. This function calculates the neighborhood overlap (Jaccard index) between every cell and its k.param nearest neighbors.[63] The graph was partitioned into clusters using the FindClusters function with different values for resolution parameter. The differential expressed gene markers for each cluster were found using the FindAllMarkers function with the option of only returning positive markers and a minimal fraction of cells with the marker of 0.25. The default Wilcoxon Rank-Sum test was used to calculate statistical differences in each cell cluster.

Cell type annotation

To delineate specific cell types within the data, cell type labels were assigned manually to clusters emerging from UMAP analysis. This annotation process was guided by the expression profiles of a set of marker genes, which are characteristic of various cell types including T cells, B cells, natural killer (NK) cells, monocytes, dendritic cells (DCs), myeloid-derived suppressor cells (MDSCs), megakaryocytes, red blood cells (RBCs), $CD34^+$ stem cells, granulocytes, lymphocytes, macrophages, basophils, eosinophils, and neutrophils. The marker genes utilized for this purpose encompassed a wide array of immune response and cell differentiation indicators such as *CD3D*, *CD3E*, *ID3*, *IL7R*, *CCR7*, *ITGB1*, *CD95*, *TCF7*, *CD3D*, *CD3E*, *CD4*, *S100A4*, *CCR10*, *FOXP3*, *IL2RA*, *TNFRSF18*, *IKZF2*, *CTLA4*, *IL2*, *IL4*, *IL13*, *IL17A*, *CD3D*, *CD3E*, *CD8A*, *CD8B*, *CCL4*, *GZMA*, *GZMB*, *GZMH*, *GZMM*, *GZMK*, *IFNG*, *GNLY*, *TNF*, *PDCD1*, *LAG3*, *CD79A*, *CD79B*, *CD19*, *JCHAIN*, *GNLY*, *NKG7*, *CD16*, *NCAM1*, *KIR2DL4*, *SIGLEC7*, *CD14*, *LYZ*, *S100A8*, *S100A9*, *LGALS3*, *FCN1*, *FCGR3A*, *MS4A7*, *FCER1A*, *CST3*, *ITGAM*, *ITGAX*, *CLEC10A*, *CLEC9A*, *THBD, CD1C, LILRA4, CLEC4C, TLR7, TLR9, ITGAM, CD33, CD3D, CD3E, CD14, CD19, FUT4, CEACAM1, HLA-DRA, HLA-DRB1, HLA-DRB5, PPBP, PF4, ITGA2B, ITGB3, PEAR1, CD42D, CD59, HBG1, HBG2, HBB, CD34, CCR3, CD11b, CD13, CD18, CD229, CRACC, CD14, CD68, CD36, CD164, LAMP1, CD44, CD69, EMR1, MPO, CD62L, CD3D, CD3E, CD4, CD8A, CD8B, NKG7, GNLY, CD14, LYZ, FCER1A, CLEC10A, LILRA4, CLEC4C, CD79A, CD79B, HBB, PPBP, PF4*. T cells were further divided into clusters to annotate subpopulations: Naive CD4, Central Memory CD4, Central Memory CD8, Anergic CD4, Activated CD4, Treg, Exhausted CD4, Stem-like CD8, NKT, Exhausted CD8, Effector CD8, Naive CD8, Cytotoxic CD4 and Effector Memory CD8 using the following marker genes: *CD3D, CD4, CD8A, CTLA4, PDCD1, TIGIT, FOXP3, CCR7, GZMK, GZMB, GZMH, IL7R, CCL5, KLRB1, TRAV16, TRAV17, CX3CR1, CCL4, TRDC, CD69, FOS, BATF, IL2RB, TBX21, EOMES, PRDM1, ICOS*.

UMAP showing pathway activity

We focused specifically on T cells. The objective was to examine the pathway activity within these T cells across various patient timepoints. This involved calculating the mean expression levels of genes associated with each pathway, a method analogous to that used in bulk RNA sequencing data analysis. The mean expression levels were then normalized against the baseline time (Pre-TTF), facilitating the observation of dynamic changes in pathway activity. The UMAP visualizations were generated using the FeaturePlot function in the Seurat package.

Violin plot showing pathway activity

Pathway activity was quantified using the same methodology as described for the UMAP analysis. This approach also incorporated additional data points, specifically the number of cells present at each timepoint and the statistical significance (*p*-value) of expression changes between timepoints compared to the Pre-TTF baseline. The significance levels were determined using the FindMarker function of the Seurat package, which assesses differential expression.

TCR clonotyping

Sample processing

The Human V(D)J Amplification Kit (10x Genomics) Single-cell RNA-seq libraries were generated using the Chromium Next GEM Single Cell 5′ v2 (Dual Index) alongside the Human V(D)J Amplification Kit (10x Genomics), following the manufacturer's protocols. To ensure consistency, all patient samples and the corresponding libraries were processed simultaneously in a single batch. Sequencing of the single-cell libraries was performed on an Illumina NovaSeq system, utilizing an 8-base i7 sample index read, a 28-base read 1 for capturing cell barcodes and unique molecular identifiers (UMIs), and a 150-base read 2 for the mRNA insert.

Data processing

The 5′ Single Cell TCRα/β V(D)J library data was first processed using 10X Genomics Cell Ranger package (v. 7.0.0, with java/9.0.1, bcl2fastq/2.20.0.422 dependencies). Command cellranger mkfastq was used to convert the raw sequencing data from the bcl to fastq format, and cellranger multi command to align to the reference genomes GRCh38 (GENCODE v.24) and single cell clonal identification. Clonal tracking plots were created using the Immunoarch R package v0.9.0 (https://cloud.r-project.org/web/packages/immunarch/index.html) with the function trackClonotypes, option col = ”a.a”, to collapse all clones that share the same amino acid sequences. TCRβ clones of immune cells from bulk primary and recurrent tumor samples were analyzed by ImmunoSeq proprietary pipeline of Adaptive Biotech. A clonal tracking grid was generated for CD8 and CD4 T Cells. In the grid, all TCRβ clones were identified at a particular timepoint and then tracked (number of cells, cell type change, pathway activity, *etc.*) for each timepoint. For example, the first row tracks all TCR clones at timepoint Pre-TTF, second row tracks all TCRβ clones at the next timepoint, and so on. The same was done for top 2 clones instead of all clones for an in-depth look.

TCR clonotyping, diversity, and evolution

A key part of this analysis involved tracking the evolution and activation of TCRβ clones over time. A clonal tracking grid was established to map the presence and characteristics of TCR clones at each patient timepoint, focusing on aspects such as the number of cells, changes in cell type, and pathway activity. For example, the first row in the grid tracks all TCR clones at timepoint Pre-TTF, second row tracks all TCRβ clones at the next patient timepoint, and so on. This tracking was performed for all identified clones, with a detailed analysis for the top two clones, offering insights into the dynamic nature of T cell responses.

Clonal diversity within the populations was quantified using the Simpson Diversity Index,[28] represented by the formula: $D = 1 - \sum_{i=1}^{n} (p_i)^2$

where p_i is the proportion of the i-th clone in the population, and n is the total number of clones observed. This index measures the probability that two randomly selected individuals from the population will be of the same clone, with values ranging from 0 (no diversity) to 1 (maximum diversity).

To evaluate changes in clonal diversity across different timepoints, the Clonal Diversity Ratio was calculated as follows: $\textit{Clonal Diversity Ratio} = \frac{D_{timepoint\ 2}}{D_{timepoint\ 1}}$

This ratio provides a comparative measure of clonal diversity between two specified timepoints. A ratio greater than 1 indicates an increase in diversity, suggesting a diversification of the clonal population over time. Conversely, a ratio less than 1 reflects a decrease in diversity, pointing to a homogenization of the population. This analysis facilitates the understanding of clonal dynamics over the course of the study.

TCRβ clonal replacement ratio calculation

The TCRβ clonal replacement ratio was calculated between two time points t1 and t2 was calculated as follows. The top clones at time point 1 was tracked in the time point 2 and their proportion in t2 was recorded (t1_top clone proportion at t2). Also, the proportion of the top clones at time 2 was calculated (t2_top clone proportion at t2).

Clonal replacement = t2_top clone proportion at t2/max (t1_top clone proportion at t2, 0.001).

The small number 0.001 was added to prevent division to zero. The *p*-value for clonal replacement was calculated using Student’s T-test, with null hypothesis that the clonal replacement ratio equal 1 and the alternative hypothesis is the clonal replacement ratio is greater than 1. To assess the role of TCRβ clonal replacement in patient survival, the Cox Proportional Hazards Model was created, using coxph and survfit commands in R survival package (v3.5.7) with multiple co-variates together: Age, Sex, MGMT.methylation, and with or without TCRβ clonal replacement ratio in the wt-IDH GBM only population. The Schoenfeld residuals test[64] was performed to assess the proportional hazards assumption in the Cox regression model. None of the covariates showed a significant violation of the assumption, indicating that the proportional hazards assumption holds for the model. Clonal replacement ratio was applied as a continuous variable. The Kaplan Meyer plot was calculated using median TCRβ replacement ratio to divide patients into 2 groups with low and high replacement ratio by survfit, survdiff (R survival package) and plotted using autoplot function of ggplot2 package (3.4.4). The *p*-value was calculated using log-rank test.

Correlation analysis

In the study, the relationship between various biological variables was assessed using the Pearson correlation coefficient. This statistical measure, calculated in R, quantifies the degree of linear relationship between two continuous variables. The Pearson correlation coefficient values range from −1 to +1, where +1 indicates a perfect positive linear relationship, −1 indicates a perfect negative linear relationship, and 0 signifies no linear correlation. Each correlation coefficient was accompanied by a *p*-value to assess the statistical significance of the observed correlation. Results with a coefficient close to +1 or −1 suggest a strong linear relationship, indicating that as one variable increases, the other variable also increases (positive correlation) or decreases (negative correlation) correspondingly. Conversely, coefficients near zero imply a weak or no linear relationship between the variables. This analysis provides insights into the potential interactions or independent behaviors of the variables within the dataset, guiding further investigations into their biological or clinical implications.

External dataset

We included a dataset with paired tumor tissues from 12 newly diagnosed GBM patients obtained before and after treatment with standard chemoradiation (n = 6) or with TTFields + chemoradiation (n = 6) (Table S5) to determine whether the changes in the

TME, including the upregulation of alternative immune checkpoints were observed without pembrolizumab. The data, accessible through the European Genome-phenome Archive (EGAC00001002176), was obtained with approval from the investigators.[53] We processed the FASTQ data using the same pipeline employed for our bulk RNA-seq analyses. The resulting TPM data was then utilized for a comparative analysis of gene expression.

Immunohistochemistry

IHC was performed in the USC Immunohistochemistry R&D Laboratory using 5-μm sections of formalin-fixed paraffin-embedded specimens. Slides were run on a Leica Bond III Autostainer. EDTA (High pH 9.0, for LGALS9 and PD-L1) and citrate (low pH 6.0, for VSIR), were used to retrieval antigen. The slides were then incubated with correlated antibodies for 15 min followed by BOND IHC Polymer Detection Kit (Leica, Cat#DS9800): anti-LGALS9 (Sigma-Aldrich, Cat#MABT833, 1:850 dilution; RRID: AB_3696950), anti-PD-L1 (Abcam, Cat#AB205921, 1:100 dilution; RRID: AB_2687878), and anti-VSIR (Abcam, Cat#AB300042. 1:100 dilution; RRID: AB_3696949). The stains were counterstained with hematoxylin and allowed to dry before they were scanned at 40x with the Phillips FMT0095.

Med, Volume *6*

Supplemental information

Efficacy and safety of adjuvant TTFields plus pembrolizumab and temozolomide in newly diagnosed glioblastoma: A phase 2 study

Dongjiang Chen, Son B. Le, Ashley P. Ghiaseddin, Harshit Manektalia, Ming Li, Adam O'Dell, Maryam Rahman, and David D. Tran

Table S1 (related to **Figure 1): Characteristics of enrolled patients and case-matched controls from EF-14**

	ITT	Per Protocol (PP)	Matched control (EF-14)	*P*-value (PP vs Matched)	wt-IDH GBM
Age (Years)					
n	31	26	56	0.787	23
Mean (SD)	57.9 (12.98)	56.7 (13.22)	55.9 (12.11)		58.6 (12.20)
Median (range)	60.7 (31-79)	60.5 (31-79)	56.5 (26-83)		60.8 (31-79)
Sex, No. (%)					
Male	22 (71)	19 (73)	38 (68)	0.633	17 (74)
Female	9 (29)	7 (27)	18 (32)		6 (26)
KPS, %					
Median (range)	80 (70-90)	80 (70-90)	80 (70-90)	0.865	80 (70-90)
EOR, N (%)					
Biopsy only	9 (29)	7 (27)	15 (27)	0.979	7 (30)
Maximal resection	22 (71)	19 (73)	41 (73)		16 (70)
MGMT status, N (%)					
Methylated	10 (32)	7 (27)	14 (25)	0.853	6 (26)
Unmethylated	21 (68)	19 (73)	42 (75)		17 (74)
IDH mutation, N (%)					
Positive	4 (13)	3 (12)	7 (12)	0.901	0 (0)
Negative	27 (87)	23 (88)	49 (88)		23 (100)
TTF usage–First 6m					
Mean % (range)	70.6 (0-95)	80.3 (55-95)	80.9 (50-94)	0.196	84.5 (55-95)

Table S2 (related to **Figure 1**): **Characteristics of patients evaluable for Safety**

Age (Years)	
n	28
Mean (SD)	57 (12.93)
Median (range)	60.5 (31-79)
Sex, No. (%)	
Male	20 (71)
Female	8 (29)
Karnofsky Performance Score, %	
Median (range)	80 (70-90)
Extent of Resection, N (%)	
Biopsy only	8 (29)
Maximal resection	28 (71)
MGMT Promoter Methylation, N (%)	
Methylated	8 (29)
Unmethylated	20 (71)
IDH-1/2 Mutation Status (by IHC/NGS), N (%)	
Positive	4 (14)
Negative	24 (86)
Dexamethasone dose at enrollment, mg daily	
Median (range)	0 (0-4)
TTFields compliance – first 6 months	
Median % (range)	84 (45-95)
TMZ cycles completed	
Median (range)	9 (1-12)
Pembrolizumab doses completed – first 6 months	
Median (range)	8.0 (0-8)

Table S3 (related to Figures 1-7): Inventory of tissue samples for multi-omics analysis in the 2THETOP study.

			PBMC scRNA-seq and TCR clonotyping								
Pt No	EOR	IDH1/2 mutation	Pre-TTF	Post-TTF (C1)	C2	C4	C9	C17	C34	R1	R2
1	Resection	positive	Samples from first 2 time points failed Q/C due to excessive degradation from PBMC cryopreservation issue. Without these baseline control samples, samples from later time points were not processed to include in the analysis.								
2	Resection	negative									
3	Biopsy	negative									
4	Biopsy	negative									
5	Resection	negative									
6	Resection	negative	○	○	⊗	○	○				
7	Biopsy	negative	○	○	○	○	○	○	○		
8	Resection	negative	○	○	○	○					
9	Resection	negative	○	○	○	○					
10	Biopsy	negative	○	○	○	○	○	○	○	○	
11	Resection	negative	○	○	○	○					
12	Biopsy	negative	○	⊗	○	○	○	○	○	○	○
13	Resection	positive	○	○	○	○					
14	Resection	negative	○	○	○	○	○	○		○	
15	Biopsy	negative	○	○	○	○					
16	Biopsy	negative	○	○	○	○					
17	Resection	negative	○	○	○	○					
18	Resection	negative	○	○	○	○					
19	Resection	negative	○	○	○	⊗					
20	Resection	positive	○	○	○	○					
21	Resection	negative	○	○	○	○	○	○		○	
22	Resection	negative	○	○	○	○	○			○	
23	Resection	negative	○	○	○	○					
24	Resection	negative	○	○	○	○	○				
25	Resection	negative	○	○	○	○					
26	Resection	negative	○	○	○	⊗	○				

Enriched T cells PBMC scRNA-seq								
Pre-TTF	Post-TTF (C1)	C2	C4	C9	C17	C34	R	R2
Samples from first 2 time points failed Q/C due to excessive degradation from PBMC cryopreservation issue. Without these baseline control samples, samples from later time points were not processed to include in the analysis.								
○	○	⊗	○	○				
○	○	○	○	○	○	○		
○	○	○	○					
○	○	○	○					
○	○	○	○	○	○	○	○	
○	○	○	○					
○	○	⊗	○	○	○	○	○	○
○	○	○	○					
○	○	○	○	○	○		○	
○	○	○	○					
○	○	○	○					
○	⊗	○	○					
○	○	○	○					
○	○	○	⊗					
○	○	○	○					
○	○	○	○	○	○		○	
○	○	○	○	○			○	
○	○	○	○					
○	○	○	○	○				
○	○	○	○					
○	○	○	⊗	○				

			Tumor WES			Tumor bulk RNA-seq			Tumor TCR clonotyping		
Pt No	EOR	IDH1/2 mutation	Primary	R1	R2	Primary	R1	R2	Primary	R1	R2
1	Resection	positive	○			○			○		
2	Resection	negative	○	○		○			○	○	
3	Biopsy	negative	○			○			○		
4	Biopsy	negative	○			○			○		
5	Resection	negative	⊗			⊗			⊗		
6	Resection	negative	○	○		⊗	○		○	○	
7	Biopsy	negative	○			⊗			○		
8	Resection	negative	○			○			○		
9	Resection	negative	○	○		○	○		○	○	
10	Biopsy	negative	○			⊗			○		
11	Resection	negative	○	○		○	○		○	○	
12	Biopsy	negative	○	○	○	○	○	○	○	○	○
13	Resection	positive	○			○			○		
14	Resection	negative	○	○		○	○		○	○	
15	Biopsy	negative	○			○			○		
16	Biopsy	negative	⊗			⊗			⊗		
17	Resection	negative	○	○		○	○		○	○	
18	Resection	negative	⊗			⊗			⊗		
19	Resection	negative	○	○		○	○		○	○	
20	Resection	positive	○			○			○		
21	Resection	negative	○	○		○	○		○	○	
22	Resection	negative	○			○			○		
23	Resection	negative	○			○			○		
24	Resection	negative	○	○		○	○		○	○	
25	Resection	negative	○			⊗			○		
26	Resection	negative	○			○			○		

○ Passed Q/C
⊗ Not obtained or failed Q/C
R1 First recurrence
R2 Second recurrence
EOR Extent of resection

Table S4 (related to **Figure 1): Toxicity Summary–Including All Treatment Related Adverse Events**

Toxicity Category	CTCAE Toxicity Term	Number of patients with Toxicity Grade Observed		
		Grade 1-2	**Grade 3**	**Grade 4**
Allergy/Immunology	Allergic reaction/hypersensitivity	1		
Blood/Bone Marrow	Thrombocytopenia	12	1	1
Coagulation	Thrombosis	2		
Constitutional Symptoms	Weight loss	6		
	Fatigue (asthenia, lethargy, malaise)	13	6	
	Fever (in the absence of neutropenia defined as ANC <1.0 x 10e9/L)	1		
	Rigors/chills	1		
Dermatology/Skin	Rash (scalp irritation)	22		
	Pruritus/itching	14		
	Dermatology/Skin - Other (Specify, __)	4		
	Rash – Other (acne/acneiform)	3		
	Urticaria (hives, welts, wheals)	1		
	Bruising (in absence of Grade 3-4 thrombocytopenia)			1
Gastrointestinal	Nausea	29		
	Vomiting	14	1	
	Diarrhea	6		
	Constipation	5		
	Taste alteration (dysgeusia)	1		
	Anorexia	1		
	Gastritis (including bile reflux gastritis)	1		
Lymphatics	Edema: limb	2		
	Edema: head and neck	1		
Metabolic/Laboratory	Bilirubin (hyperbilirubinemia)	1		
	ALT, SGPT (serum glutamic pyruvic transaminase)	2	1	
Musculoskeletal/Soft Tissue	Extremity-lower (gait/walking)	6		
	Joint effusion	2		
	Muscle weakness, generalized or specific area (not due to neuropathy) - Extraocular	3	1	
Neurology	Dizziness	1		
	Memory impairment	2		
	Mood alteration - Anxiety	1		
	Neurology - Other		1	2
	Personality/behavioral	1		
	Speech impairment (e.g., dysphasia or aphasia)	5		
Pain	Pain-Head/headache	8		
	Pain-Extremity-limb	8		
	Pain-Scalp	6		
	Pain-Joint	3		
	Pain-Abdomen NOS	2		
	Pain-Other		1	
	Pain-Stomach	1		
	Pain-Muscle	1		
	Pain- Lymph node	1		
Renal/Genitourinary	Incontinence, urinary	1		

Table S5 (related to **Figure 7D): Patient characteristics of the control cohort from Diamant et al. J Immunol (2021)**

Group	Patient no.	Sex	Age (years)	PFS (days)
TMZ alone	8	F	62	806
	9	F	57	281
	11	M	59	548
	13	M	61	222
	16	F	59	634
	17	M	52	544
TMZ+ TTF	1	F	32	614
	2	F	59	311
	3	M	57	514
	4	M	58	176
	5	F	61	427
	6	M	47	88

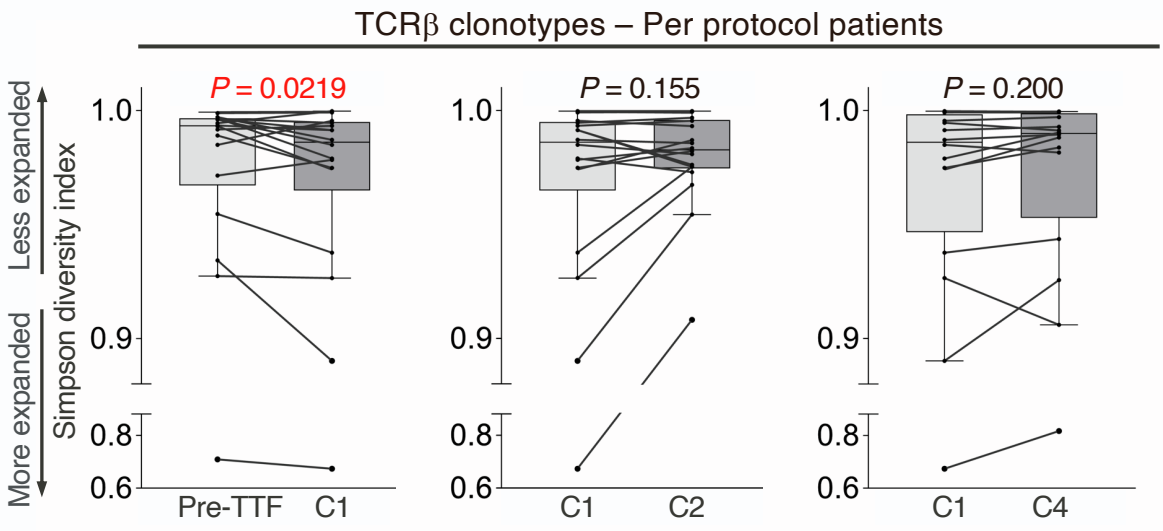

Figure S1 (related to **Figure 3A): TCRβ clonotyping in PP patients.**

Combo box-and-whisker and dot plots illustrating TCRβ clonal diversity, calculated using the Simpson's diversity index, across different treatment periods in individual PP patients, confirming significant TCRβ clonal expansion associated with TTFields treatment, whereas pembrolizumab administration did not induce TCR clonal expansion. N=19.

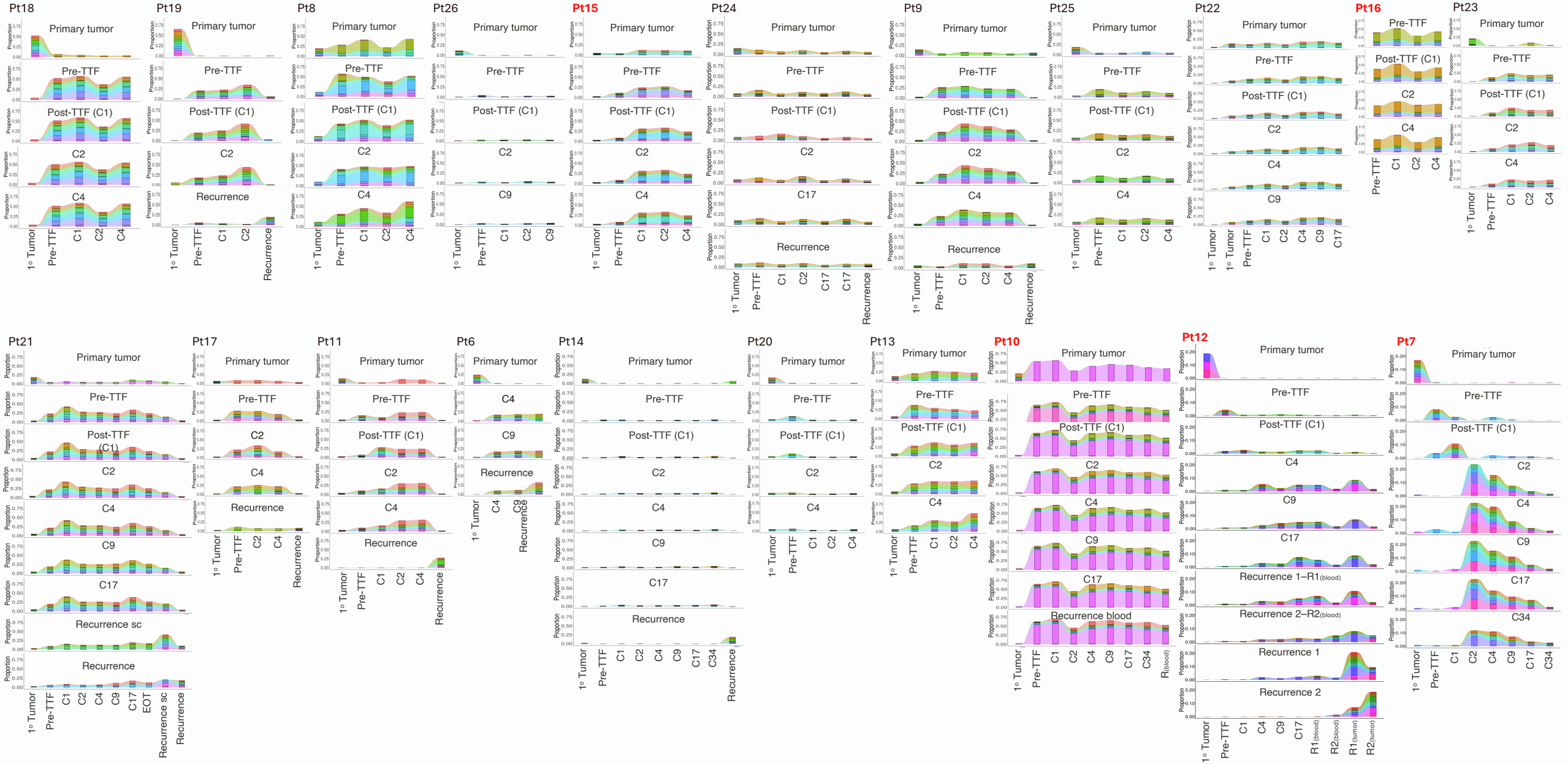

Figure S2 (related to **Figure 3B):** Tracking the top 10 most expanded TCRβ clones at each treatment timepoint for all PP patients, ordered by survival duration from shortest to longest (left to right, top to bottom). Patients in bold red font are biopsy-only.

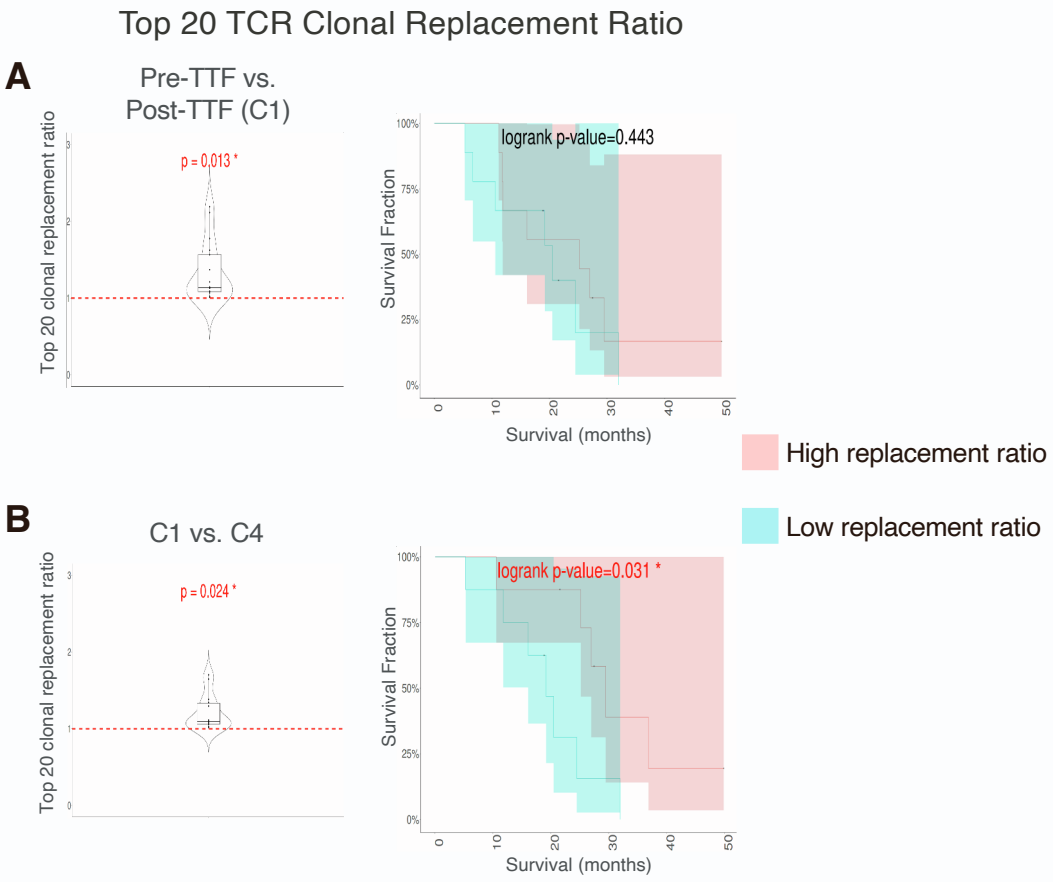

Figure S3 (related to **Figure 3C-D): Top 20 TCRβ clonal replacement between various treatment periods in wt-IDH GBM population.**

(Left) Violin plots of top 20 TCRβ clonal replacement ratio between Pre-TTF vs Post-TTF (C1) (**A**) and between C1-C4 (**B**).

(Right) Kaplan Meier plot using low or high top 20 TCRβ clonal replacement ratio around the median in a univariate analysis between Pre-TTF vs Post-TTF (C1) (**A**) and between C1-C4 (**B**). These results show that Top 20 TCRβ clonal replacement ratio between C1 and C4 is predictive of extended survival.

TCRβ clonal replacement ratio was analyzed using paired Student T-test. Survival comparison was assessed using log rank test.

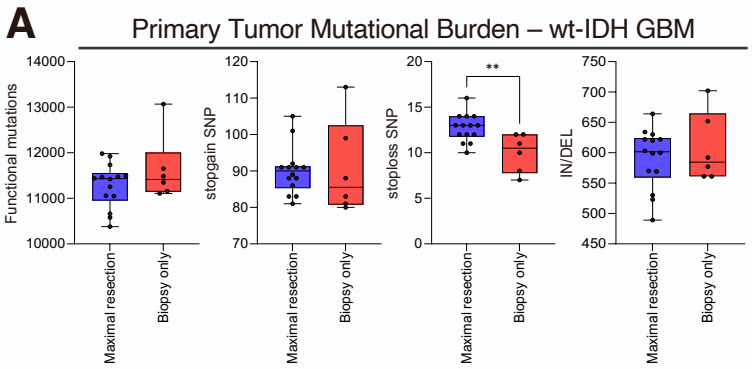

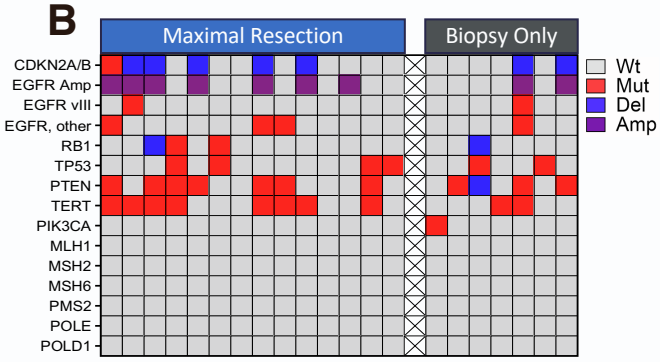

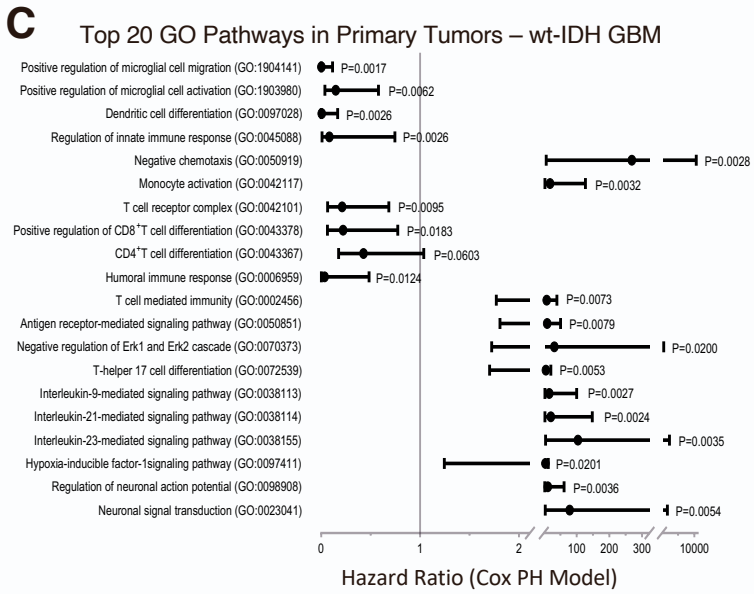

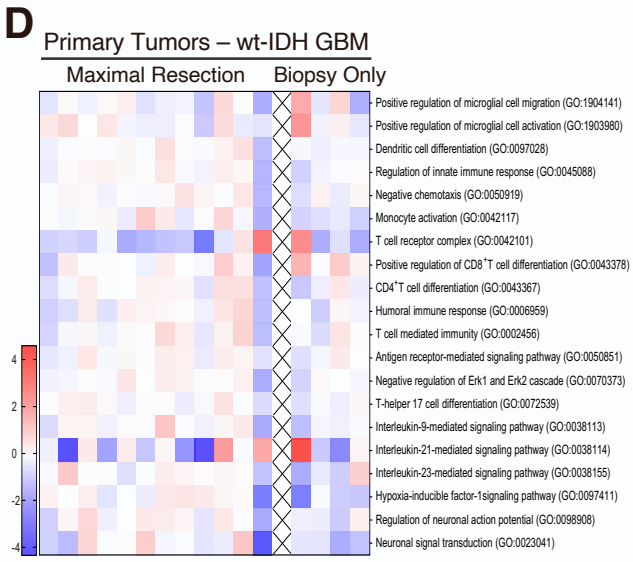

Global Network Changes in Enriched T cells – wt-IDH GBM: Maximal Resection vs Biopsy Only

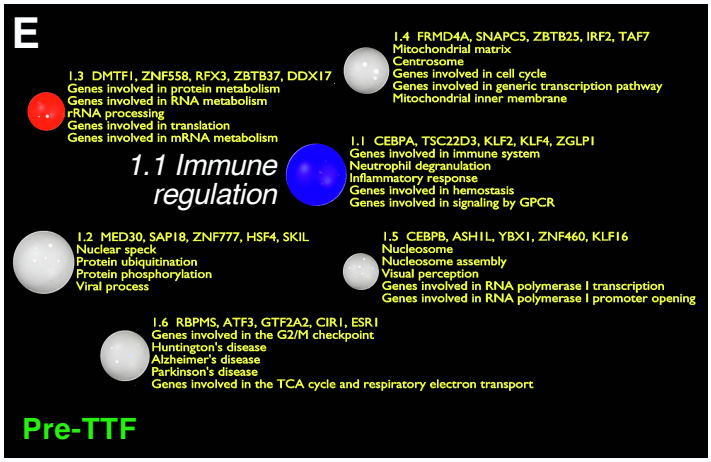

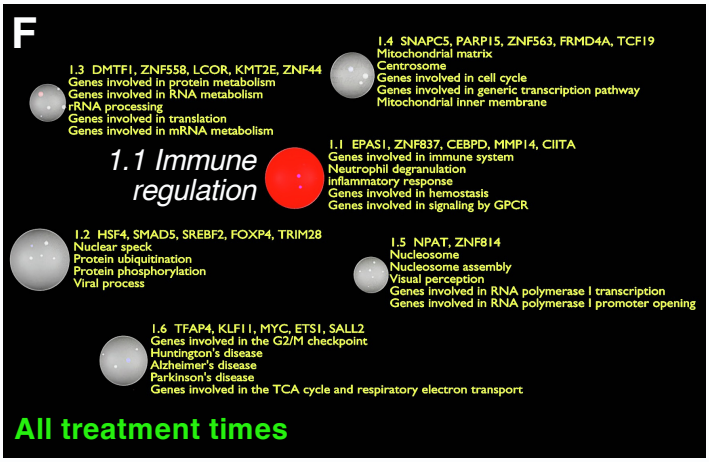

Figure S4

Figure S4 (related to **Figures 4-6): Patients with maximal resection and biopsy-only wt-IDH tumors show similar TME characteristics in primary tumors and systemic T cell activity at study entry.**

A) Combo box-and-whisker and dot plots illustrating total functional mutational burden, stop-gain SNP, stop-loss SNP, and insertions/deletions (IN/DEL), revealing minimal differences in tumor mutational burden between maximal resection and biopsy-only primary tumors in the wt-IDH GBM population. N=14, maximal resection; N=6, biopsy-only. Data are represented as mean ±SEM. The whiskers are the minimum and maximum values, the lower and upper box edges the 25th and 75th percentage values, respectively, and the lines within the boxes the median. Comparisons were performed using unpaired Student's T-test with a 2-tailed distribution. *, $P<0.05$; **, $P<0.01$.

B) Mutations (Mut) and copy number variation (deletion [Del] or amplification [Amp]) profiles of genes with known prognostic or predictive significance in high-grade glioma and immune-oncology in primary maximal resection and biopsy-only tumors, revealing a similar distribution of genetic alterations between the 2 groups. N=14, maximal resection; N=7, biopsy-only.

C) Multivariate Cox PH model analyzing 20 GO immune pathways most strongly associated with survival in primary wt-IDH GBM tumors. N=12, maximal resection; N=4, biopsy-only.

D) Heatmap showing the mean expression levels of the 20 GO pathways most strongly correlated with survival in primary wt-IDH tumors revealed no significant differences between maximal resection and biopsy-only groups. N=12, maximal resection; N=4, biopsy-only.

E-F) 3D maps of global pathway hubs generated by GeneRep/nSCORE from bulk RNA-seq data of peripheral T cells in patients with maximal resection versus biopsy-only wt-IDH GBM tumors at Pre-TTF (**E**) and all subsequent treatment time periods (**F**), illustrating that the immune activity of peripheral T cells, measured by the expression signal of immune regulatory hub 1.1, was reduced before TTFields treatment and subsequently increased after the initiation of TTFields and pembrolizumab in biopsy-only patients compared to those with maximal resection. Globe size: the number of pathways in a hub; Globe colors: Red–Upregulated in biopsy-only patients; Blue–downregulated in biopsy-only patients; Grey–No change in biopsy-only patients compared to Maximal resection patients. Gene names listed after a globe number are master regulators of that hub. N=14, maximal resection; N=5, biopsy-only.

Figure S5 (related to **Figure 6A): Representative markers for T cell cluster annotation.**

2D UMAP of expression of indicated representative markers of T cell subtypes and functions in all T cell clusters.

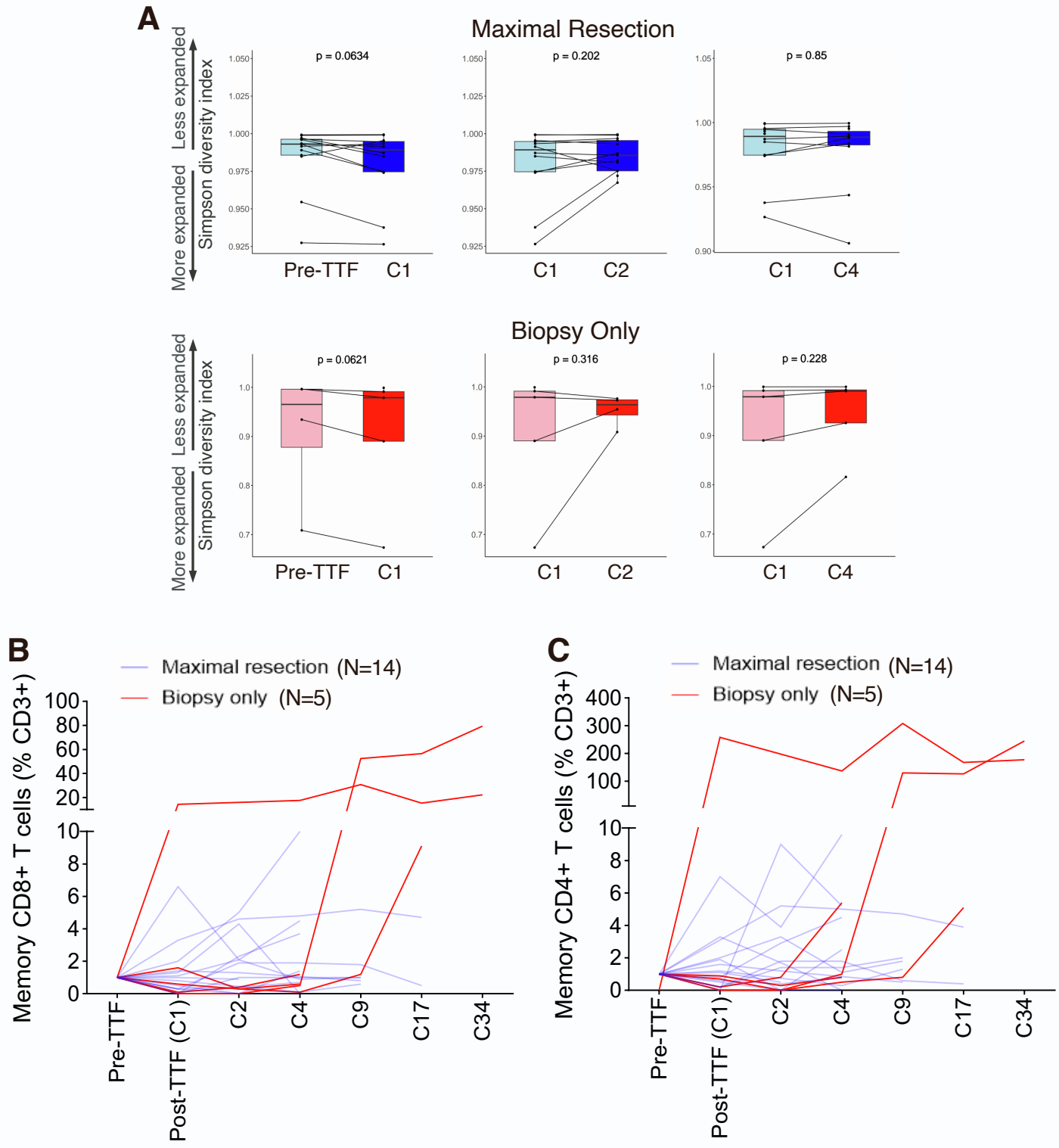

Figure S6 (related to **Figure 6D** and **Figure 6F**): **TCRβ clonotyping and central memory (CM) T cell formation in Maximal Resection vs Biopsy-Only patients.**

Combined box-and-whisker and dot plots illustrating TCRβ clonal diversity, measured by the Simpson diversity index, at various treatment periods in patients with maximal resection or biopsy-only wt-IDH GBM tumors (**A**). CM $CD8^+$ (**B**) and $CD4^+$ (**C**) T cell fractions as percentages of $CD3^+$ cells and normalized to Pre-TTF rose later in the treatment course and more persistently in biopsy-only patients, compared to those with maximal resection. N=14, Maximal Resection; N=5, Biopsy-Only

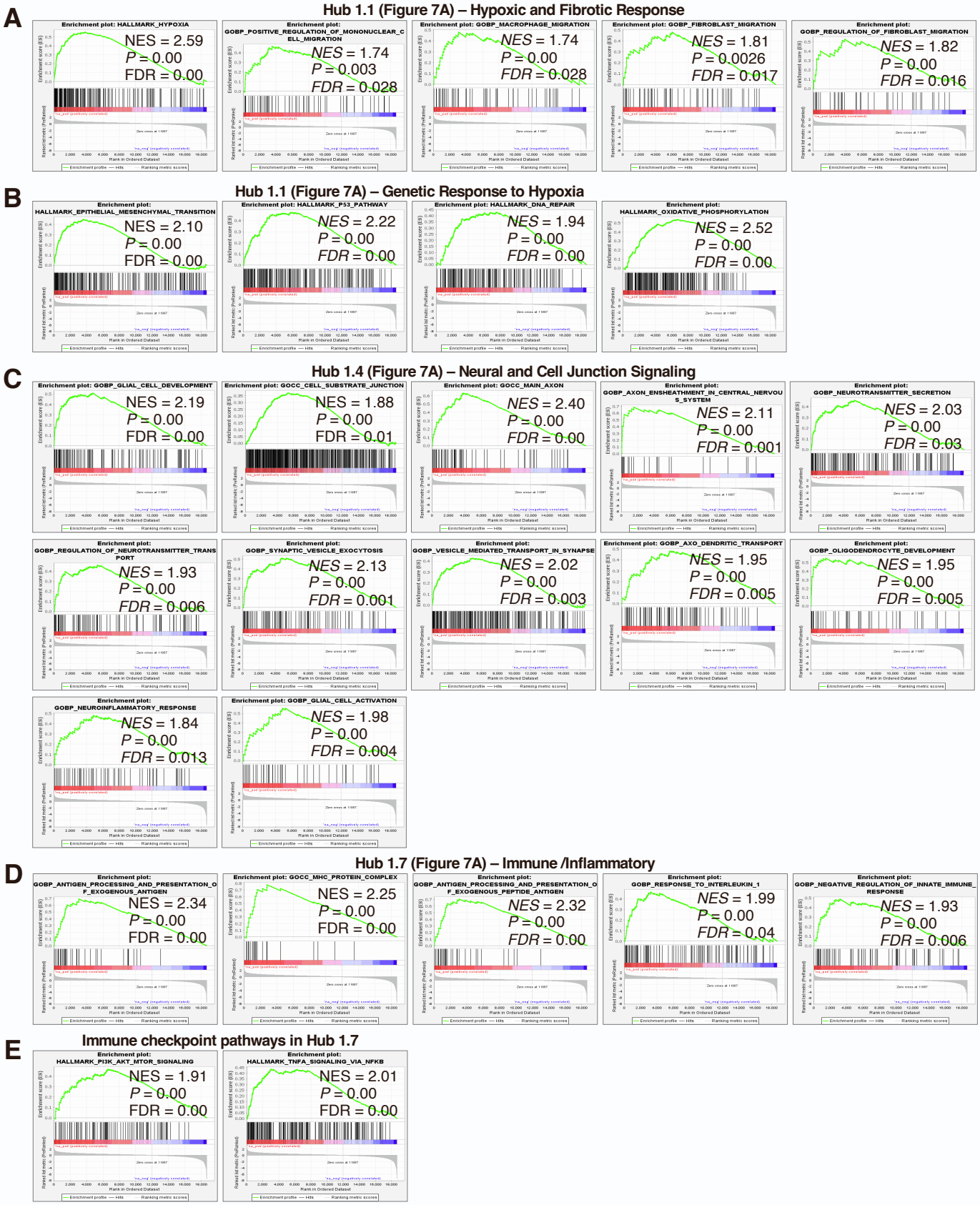

Figure S7 (related to **Figure 7A**): **TME reprogramming in recurrent wt-IDH tumors.**

GSEA of representative GO pathways in Hub 1.1, including migratory regulation (**A**) and genetic response to hypoxia (**B**), Hub 1.4, including axonic, neurotransmitter, and junctional complex signaling (**C**), and Hub 1.7, including antigen presentation and inflammatory (**D**) and immune checkpoint regulatory (**E**) pathways in 9 paired primary vs recurrent wt-IDH tumors. NES: normalized enrichment score. FDR: False discovery rate.